

424 (PB-057)

Poster

Death associated protein 3 influences heat shock protein 90 expression in breast cancer cell lines

M. Uhercik^{1,2}, A. Sanders¹, A. Sharma², K. Mokbel³, W. Jiang¹. ¹Cardiff University, Cardiff China Medical Research Collaborative CCMRC, Cardiff, United Kingdom; ²St George's University Hospital, Breast Surgery, London, United Kingdom; ³Princess Grace Hospital, The London Breast Institute, London, United Kingdom

Background: Death Associated Protein 3 (DAP3) is involved in programmed cell death and is believed to have proapoptotic and antioncogenic effects. In breast cancer a strong inverse correlation between DAP3 and tumour grade, Nottingham Prognostic Index, clinical stage, and clinical outcome has been identified. The Heat Shock Protein 90 (HSP90) and its 2 isoforms (HSP90a and HSP90b) are chaperone proteins that interact with a great number of other proteins called clients, modulating the activity of many biochemical pathways. Previous work undertaken in our laboratories has suggested an interaction between DAP3 and HSP90 in human breast cancer. In the current study we aim to further elucidate the relationship between DAP3 and HSP90.

Material and Methods: DAP3 expression was knocked down in MCF7 and MDA-MB-231 breast cancer cell lines using ribozyme transgene technology and verified at the transcript level using quantitative polymerase chain reaction (qPCR). Subsequently the expression pattern of HSP90 was examined at the transcript and protein level, using qPCR and Western blotting respectively, in the MCF7 and MDA-MB-231 knockdown cell lines. To explore a potential influence of HSP90 inhibition on DAP3 expression, HSP90 small molecule inhibitor was used to treat wild type MCF7 and MDA-MB-231 cell lines in time and concentration gradient and DAP3 expression levels were examined using qPCR.

Results: DAP3 knockdown was demonstrated in both MCF7 and MDA-MB-231 cell lines (both $p < 0.05$) and was also indicated at the protein level, though this was more apparent in MCF7 cells. qPCR highlighted a significant decrease of HSP90a expression in MCF7 DAP3 KD cells ($p = 0.05$) and a similar trend was seen for HSP90b expression, though this was not found to be statistically significant ($p = 0.089$). A significant decrease in HSP90b expression was seen in MDA-MB-231 expression following DAP3 knockdown ($p = 0.013$) and a similar trend was seen for HSP90a expression, though this was not quite significant ($p = 0.06$). MCF7 and MDA-MB-231 wild type cells treated with HSP90 inhibitor did not demonstrate any differences in DAP3 expression levels over a range of time points or concentration gradient.

Conclusions: This is the first time the link between DAP3 and HSP90 has been described in human breast cancer. Our results indicate that DAP3 may play an important role in modulating the expression of HSP90a and HSP90b and give more insight into DAP3 downstream effectors. Our group is currently further evaluating the functional effects of these findings.

No conflict of interest

425 (PB-058)

Poster

The evaluation of the influence of preoperative Metformin to TILs and ALDH1 expression of breast cancer.

T. Takahiro. Okayama Univ, Biopathological Science, Okayama, Japan

Background: There are some reports about the prognostic effects of immune function. Metformin is one of the most commonly prescribed drugs for type 2 diabetes, and previous studies have reported that metformin has an anti-tumor effect according to the improvement of the immune function. On the other hands, Aldehyde dehydrogenase 1 (ALDH1) and tumor infiltrating lymphocytes (TILs) are known to be prognostic factors and predictive markers of chemosensitivity. There is no report about the influence of Metformin to these markers.

Patients and Methods: This is the ancillary study of the prospective study (UMIN00014689). 17 breast cancer patients who took a daily dose of metformin orally for 7–21 days before surgery. To determine the efficacy of metformin, TILs, ALDH1 expression and other prognostic markers in both specimens from core needle biopsy before treatment and surgery were evaluated.

Results: Median age was 57 (36–74). 15 patients could take metformin for 2 weeks before surgery, and 2 patients stopped because of nausea. The breast cancer subtype was luminal A type (ER+, HER2-, Ki67 < 15%); 6 (35%), Luminal B type (ER+, HER2-, Ki67 > 15%); 5 (30%), Luminal HER2 type; 1 (6%) and Triple negative type; 5 (30%). The breast cancer with TILs were 2 (12%) in CNB specimens before metformin and 5 (30%) in surgical specimen. The expression of ALDH1 increased from 1 (6%) to 8 (48%) patients before and after metformin, and ALDH1 in 4 patients changed to strongly positive.

Conclusion: The expressions of TILs and ALDH1 were changed by preoperative metformin. The metformin may have the efficacy of

improvement of chemosensitivity from this preliminary study. The prospective trial is needed to confirm this hypothesis.

No conflict of interest

427 (PB-060)

Poster

Comparative analysis of mesenchymal stem cells from bone marrow, adipose tissue and decidua fetal membrane as sources for cell therapy in breast cancer

S. Kazemi¹, B. Sadeghi², N. Aghdami³, K. Parivar⁴, L. Farahmand⁵. ¹Breast Cancer Research Center- Motamed Cancer Institute- Acecr- Tehran, Iran; ²Cancer Immunotherapy And Regenerative Medicine Department, Tehran, Iran; ³Breast Cancer Research Center- Motamed Cancer Institute- Acecr, Cancer Immunotherapy And Regenerative Medicine, Tehran, Iran; ⁴Royan Institute, Regenerative Biomedicine And Cell Therapy, Tehran, Iran; ⁵Faculty of Basic Sciences- Science And Research Branch- Islamic Azad University, Department of Biology, Tehran, Iran; ⁶Breast Cancer Research Center- Motamed Cancer Institute- Acecr, Recombinant Proteins Department, Tehran, Iran

Introduction: Bone marrow or adipose derived mesenchymal stromal cells (BM-MSC or Ad-MSC) are widely used in several clinical disorders. However due to the invasive isolation procedure and limited efficacy in some reports finding new sources of stromal cells with easier isolation method and more potent in efficiency is major interest. Decidua stromal cells (DSCs) isolates from placenta after delivery with no or limited ethical issue and potent immunosuppressive effect in clinical setting. In this study phenotypical and functional properties of BM-MSC and Ad-MSC were analyzed and compared with DSCs.

Method: Bone marrow and adipose derived stromal cells were isolated from two patients and volunteer. DSC were isolated from 2 placentas. Isolated MSCs were expanded until passage 11. Immunophenotype analysis using flow cytometry, multi-lineage differentiation capacity assay and proliferation capacity were compared.

Results: BM-MSC were the most and DSCs were the least potent stromal cells in osteogenic, adipogenic, and chondrogenic differentiation potential while Ad-MSC were in the middle. DSCs showed the highest proliferation potential in comparison to BM-MSC and Ad-MSC. Moreover, DSCs expressed highest level of CD105, CD90, CD75 and CD44 as compared to BM-MSC and Ad-MSC.

Conclusion: We have found that DSCs fulfill all necessary criteria as stromal cells, while show better expansion capacity, easier isolation method and no or limited ethical issues. Therefore DSCs could be a better candidate for stromal cell therapy especially in inflammatory disorders.

No conflict of interest

428 (PB-061)

Poster

Elucidating Therapeutic potential of Bauhinia variegata L. using breast cancer cell line

S. Purani, P. Robin, S. Dave. The Maharaja Sayajirao University of Baroda, Department of Biochemistry, Vadodra, Gujarat, India

Background: Global cancer burden has continued its upward trend in spite of advances in research, with a marked increase of 1.67 million new breast cancer cases and death of 5.2 lakh females. In India, incidence rate of breast cancer is 1.4 lakhs whereas the mortality rate is around 70 thousand. In developing countries, financial and social reasons add to this abysmal trend. Hence, key to the effective treatment is the identification of chemotherapeutic agents that can be effective against cancer progression apart from being cost effective. Ayurvedic pharmacopoeia describes the vital role played by medicinal plants against many diseases including cancer. The contemporary world is looking for more plant-derived compounds with more efficacy against various types of cancer. *Bauhinia variegata* L. has emerged as a plant with anti-oxidant and immunomodulatory potential which can be exploited to modulate its effect on breast cancer cells. Methanolic extracts of *Bauhinia variegata* showed anticarcinogenic and antimutagenic properties in swiss albino mice induced with Dalton ascetic lymphoma, DMBA induced skin carcinogenesis and liver tumour. The proposed study has been aimed to evaluate the role of phytochemicals from *Bauhinia variegata* against breast cancer cell-lines with the emphasis to understand its molecular mechanism of action which has not been elucidated till date.

Material and Methods: Human breast cancer cells (MCF-7) were procured from NCCS, Pune, India. Cultures were maintained according to standard protocols. Plant extract was dissolved in DMSO (<0.1%). MTT assay was performed to check the cytotoxic effect of the extract. Effect of TNF- α was tested on MCF-7 cells in presence and absence of the extract.

Spheroids (in-vitro tumors) were generated as they mimic both architecture and share the same characteristics as tumor cells. Cell Migration and Invasion assay was also carried out to check the effect of extract on migratory properties of cells.

Results: It was observed that the extract had cytotoxic effect on MCF-7 cells. Moreover, extract treated cells showed changes in cell morphology. There was no effect of TNF- α on cell proliferation but significant decrease was seen when the cells were treated with extract in presence of TNF- α . Decreased colonization was observed in treated cells in dose dependent manner compared to that of control cells. Spheroids made from extract treated cells were smaller in size compared to that of control cells. Moreover treated cells did not show luminal spaces losing their typical characteristic of mammary gland cell as shown by control cells. Treated cells have lost their invasiveness whereas control cells migrates via invadosomes.

Conclusion: This plant may have a potential to be used as alternative therapeutic agent against breast cancer leading to identification of novel drug.

No conflict of interest

429 (PB-062)

Poster

Elevated Bcl-2 expression as an independent prognostic marker for decreased overall survival in patients with triple-negative breast cancer

L. Beketic Oreskovic¹, P. Ozretic², I. Alvir³, Z. Vujaskovic⁴, Z. Rendic-Miocevic¹, A. Roguljic¹, B. Sarcevic⁵. ¹University Hospital for Tumors, Department of Radiotherapy and Internal Oncology, Zagreb, Croatia; ²Rudjer Boskovic Institute, Division of Molecular Medicine, Zagreb, Croatia; ³University Hospital for Tumors, Department of Gynecologic Oncology, Zagreb, Croatia; ⁴University of Maryland School of Medicine, Department of Radiation Oncology, Baltimore, USA; ⁵University Hospital for Tumors, Department of Pathology, Zagreb, Croatia

Background: Triple-negative ductal invasive breast cancer (TNBC) shows often very aggressive behavior with a high rate of recurrence and poor survival of patients. The objective of this study was to examine the prognostic significance of carbonic anhydrase IX (CAIX), an endogenous marker for tumor hypoxia; the cellular tumor antigen p53; and the apoptosis regulator Bcl-2, in TNBC patients.

Material and Methods: Immunohistochemically determined expression of CAIX, p53, Bcl-2 and cellular proliferation marker Ki-67, analyzed in 64 formalin-fixed, paraffin-embedded TNBC tissue samples, was used to assess the relation of those markers to clinicopathological variables and prognostic implications for overall survival (OS).

Results: Bcl-2 expression was negatively correlated with histological tumor grade, while expression of p53 was positively correlated with the same clinical variable (P = 0.036 and P = 0.033, respectively). The p53 expression was also positively correlated with tumor size (P = 0.010). Survival analysis showed that patients with high Bcl-2 expression (above the cutoff value determined by receiver operator characteristic [ROC] curve analysis) had shorter OS (P = 0.020). The same was observed for patients with tumors larger than 50 mm (P = 0.034) or positive lymph nodes (P = 0.004). Among all four examined markers, multivariate analysis showed that only elevated Bcl-2 expression was a strong independent prognostic indicator for decreased OS (hazard ratio [HR] = 15.16, 95% confidence interval [95% CI], 2.881–79.727, P = 0.001).

Conclusions: Elevated expression of Bcl-2 was an independent prognostic maker for poorer OS in TNBC and as such a significant marker for tumor aggressiveness.

No conflict of interest

430 (PB-063)

Poster

Benzoxazolone and benzothiazolone combretastatin A-4 analogs with potential cytotoxic activity against breast cancer cell lines

G. Atanasov¹, S. Stateva¹, M. Gerova², O. Petrov², M. Apostolova¹. ¹Institute of Molecular Biology "Roumen Tsanev", Medical and Biological research Laboratory, Sofia, Bulgaria; ²Faculty of Chemistry and Pharmacy-Sofia University "St. Kliment Ohridski", Department of Pharmaceutical and Applied Organic Chemistry, Sofia, Bulgaria

Background: Combretastatin A-4 (CA-4), a natural stilbene, is microtubule-destabilizing agent, which binds to the colchicine domain on β -tubulin, and presents one of the most potent vascular disrupting agents that selectively targets and destroys tumor blood vessels. Additionally, CA-4 prove to be quite effective against breast cancer cells resistance towards certain adjuvant therapeutic drugs. Its therapeutic potential has inspired synthesis of various stilbene derivatives. In this study we have tested the activity of a set of 28 cis/

trans newly synthesized benzoxazolone and 24 cis/trans benzothiazolone analogs of CA-4 against endothelial and breast cancer cells.

Material and Methods: Library of 52 cis- and trans-styrylbenzoxazolones and styrylbenzothiazolone was obtained by a modified Wittig reaction under Boden's conditions. MTT test on two non-tumorigenic cell lines (EAhy926 and MCF10-A) and two breast cancer cell lines (MCF 7 and MDA-MB-231), was conducted to assess the anti-proliferative activity of the analogs in a concentration range from 10nM to 25 μ M. Analysis of capillary tube formation as a model of angiogenesis was assayed using Matrigel-based assay. The cell cycle was analyzed by flowcytometry. The effect of CA-4 analogs on tubulin polymerization was studied by immunofluorescence and in vitro tubulin polymerization assay.

Results: Although some of the analogs show strong cytotoxic activity against EAhy926 endothelial cells in nanomolar concentrations they are less effective than CA-4. Overall best results with the EAhy926 cell line were obtained for S19 and S7 analogues with IC₅₀ \approx 0.3 μ M. Analog and CA-4 exhibited similar inhibitory effect on the process of endothelial tube formation as seen from results obtained by angiogenesis assay, and trigger similar morphological changes. This was confirmed with the results obtained by tubulin polymerization assay and immunofluorescence. Treatment of endothelial cell line caused cell cycle arrest in G2/M phase. However, while CA-4 has an IC₅₀ = 1.17 μ M for MCF-10A control cell line, both S7 and S19 showed only weak cytostatic activity (80% alive). The IC₅₀ values against MCF7 cell line were 0.86 μ M for S19 and 0.07 μ M for S7. The corresponding IC₅₀ values for the MDA-MB-231 were 2.59 μ M for S19 and 0.17 μ M for S7, compared to the cytostatic effect of CA-4 for MCF-7 (30% alive) and MDA-MB-231 (50% alive).

Conclusions: Benzothiazolone and benzoxazolone CA-4 analogues are less effective against endothelial cell line, and may be less appropriate to be used as vascular disrupting anti-cancer agents, but they show stronger cytotoxic activity on examined CA-4 resistant breast cancer cell lines. While this results are very promising, more detailed studies should be done to evaluate this analogues potential to be used as antitumor agents.

The authors are grateful to the BAS for the financial support under Grant DFNP-17-124/2017.

No conflict of interest

431 (PB-064)

Poster

TP53 mutations in molecular subtypes of breast cancer in young pakistani patients – A clinicopathological link

N. Naseem¹, N. Mehmood², A.H. Nagi³. ¹University of Health Sciences Lahore Pakistan, Departments of Morbid Anatomy and Histopathology, Lahore, Pakistan; ²University of Health Sciences Lahore- Pakistan, Department of Biotechnology, Lahore, Pakistan; ³University of Health Sciences Lahore- Pakistan, Morbid Anatomy and Histopathology, Lahore, Pakistan

Background: The incidence and mortality of breast cancer varies significantly in geographically distinct populations. In Pakistan, breast cancer has shown an increase in incidence in young females and is characterized by more aggressive behaviour. The tumor suppressor TP53 gene is a crucial genetic factor that plays a significant role in breast carcinogenesis. This study investigated the TP53 mutations in molecular subtypes of both node negative and positive breast cancer in young Pakistani patients.

Material and Methods: p53, Estrogen Receptor (ER), Progesterone Receptor (PR), Her-2 neu and Ki 67 expressions were analyzed immunohistochemically in a series of 75 node negative (A) and 75 node positive (B) young (aged : 19–40 years) breast cancer patients diagnosed between 2015 and 2017 at INMOL Medical Centre, Lahore Pakistan. Tumour tissue specimens and peripheral blood samples were examined for Tp53 mutations by direct sequencing of the gene (exons 4–9). The relation of TP53 mutations to these markers and clinicopathological data was investigated.

Results: Mean age of the patients was 32.4 + 9.1 SD. Invasive breast carcinoma was the most frequent histological variant (A = 92%, B = 94.6%). Grade 3 carcinoma was the commonest grade (A = 72%, B = 81.3%). Triple negative cases (ER⁻, PR⁻, Her-2) formed most of the molecular subtypes (A = 44%, B = 50.6%). A total of 17.2% (A:6.6%, B:10.6%) patients showed TP53 mutations. Mutations were significantly more frequent in triple negative cases (A: 74.8%, B: 62.2%) compared to HER2-positive patients (P < 0.0001) and correlated well with the P53 IHC expression (P = 0.039). In the multivariate analysis of the whole patient group, the independent prognosticator were triple negative cases (P = 0.021), TP53 overexpression by IHC (P = 0.001) and advanced-stage disease (P = 0.007). No statistically significant correlation between TP53 mutations and clinicopathological parameters was found (P < 0.05).

Conclusions: It is concluded that TP53 mutations are infrequently present in breast carcinoma of young Pakistani population and there was no



***Bauhinia variegata* Bark Extract: Assessment of its Anti-proliferative and Apoptotic Activities on A549 and H460 Lung Cancer Cell Lines**

Tanvi Khanna, Akash Dave, Sejal Purani, Jagath Vedamurthy, Dhaval Jivani and Pushpa Robin*

Department of Biochemistry, The Maharaja Sayajirao University of Baroda, Vadodara - 390002, Gujarat, India; pushparobin@gmail.com

Abstract

The hunt for novel anticancer drugs with minimal side effects continues. This study strengthens the claim by providing biochemical evidences of anticancer activities of *Bauhinia variegata* bark extracts on lung carcinoma cells (A549 and H460). Bark extracts of *Bauhinia variegata* were prepared by different solvents using Soxhlet apparatus and tested for their antioxidant potential by DPPH assay. The lung cancer cell lines were treated with *Bauhinia variegata* bark extracts and viability of cells was measured by MTT assay; metastatic ability was determined through Scratch assay and effect on DNA integrity was shown by gel electrophoresis. The Petroleum Ether Bark Extract (PEBE) inhibits proliferation (A549, IC50 = 1.5 mg/ml) at 48 h treatment. DNA damage was observed in A549 cells by agarose gel electrophoresis. The Chloroform Bark Extract (CBE) inhibited proliferation of H460 (IC50 = 1 mg/ml) with DNA damage after 24 h treatment. Soft agar assay indicated decreased ability to form colonies and scratch test showed impaired migration of A549 and H460 to PEBE and CBE treatment respectively. Apoptosis was detected using fluorescent dye staining in A549 and H460 cells. Caspase 3 activity was increased significantly in A549 and H460 cells. PEBE and CBE decrease the mitochondrial membrane potential gradient ($\Delta\Psi_m$) of A549 and H460 cells respectively. This study categorically proves the cytotoxic activity of *Bauhinia variegata* bark extracts on A549 and H460 cells.

Keywords: Anticancer Effect, Caspase, DNA Damage, Metastasis, Non-small Cell Lung Cancer Cell Lines

Abbreviations: Non-Small Cell Lung Cancer (NSCLC), 3-(4,5-Dimethylthiazol-2-yl)-2,5-diphenyltetrazolium bromide (MTT), Petroleum Ether Bark Extract (PEBE), Chloroform Bark Extract (CBE), Petroleum Ether (PE), N-hexane (HX), Chloroform (CHL), Ethyl Acetate (EA), Methanol (MET), Water (AQ), Dimethyl sulfoxide (DMSO), 2, 2-Diphenyl-1-picrylhydrazyl (DPPH), Standard Deviation (SD), Standard Error of Mean (SEM), Dulbecco's Modified Eagle's Medium (DMEM), 2',7'-dichlorodihydrofluorescein diacetate (H2DCF-DA), Phosphate Buffer Saline (PBS), Hydrogen peroxide (H2O2), TAE (Triacetate- EDTA), Sodium Chloride (NaCl), Half Maximal Inhibitory Concentration (IC50), Tetramethyl Rhodamine, Methyl Ester (TMRM),

4',6-diamidino-2-phenylindole (DAPI), Analysis Of Variance (ANOVA), Acridine Orange (AO), Ethidium bromide (EtBr)

1. Introduction

Exponential increase in cancer incidences is a global burden. Every year India reports about 70,275 lung cancer cases (fourth among all cancers) with 50 % mortality within a year and 5-year survival has remained at 11-17 % for these lung cancer patients^{1,2}. Non-small cell lung cancer (NSCLC) contributes for about 85 % of the lung cancer cases while 15 % cases are SCLC².

*Author for correspondence

The most typical NSCLC is adenocarcinoma (40 %), followed by large cell carcinoma (15 %)³. Hence, in this study A549 (adenocarcinoma) and H460 (large cell carcinoma) cell lines were used. The 5-year relative survival rate of lung cancer has increased with time, but less than 21 %³. The poor survival rate along with low efficacy and side effects of chemotherapy (20-30 %) are major causes of concern in lung cancer⁴,⁵. The side effects related to present drugs motivates scientists to search for anticancer compounds from natural sources such as plant phytochemicals. Phytochemicals have lower toxicity providing an attractive alternative in cancer therapy⁶,⁷. Plant of our interest is *Bauhinia variegata*, a species in the legume family, Fabaceae. It is commonly known as Mountain Ebony, which is a medium-sized deciduous tree found throughout India. *Bauhinia variegata* L. has been mentioned in traditional texts to have multiple pharmacological activities⁸ with preliminary proof of *in-vitro* cytotoxic activity of leaf and bark extracts. Government of India has given a lot of emphasis on bringing its traditional ayurvedic knowledge to greater acceptability through validation using biochemical mechanisms involved⁹.

Cancer cells has increased ROS levels as compared to their normal counterparts and are detoxified by complex antioxidative mechanisms¹¹. Progression of cancer has been shown to follow changes in ROS¹⁰-¹². A fall out in Oxidative stress happens due to imbalance between the systems which generates and scavenges ROS. Cell apoptosis progresses with distinct biochemical pathways and plays a critical role in development and homeostasis¹³. Cancer cells have the ability to circumvent apoptosis making proteins involved in the apoptotic cascades as ideal targets for cancer therapy¹⁶. Reestablishing apoptotic programming in malignant cells selectively kills tumor cells and caspases as primary inducers of apoptosis provide an ideal platform to develop effective therapeutic strategies for cancer¹⁴,¹⁵. Here, we report the biochemical basis for the effective anticancer potential of *Bauhinia variegata* bark extracts on lung cancer.

2. Material and Methods

2.1 Plant Material Collection and Phytoextraction

Bauhinia variegata bark was collected from Waghai botanical garden, Dang, Gujarat during December-January each year and was validated by the Department of Botany, The Maharaja Sayajirao University of Baroda, India. The bark was washed, surface sterilized with 0.1 % mercuric chloride, rinsed - shade dried, powdered and packed into a thimble for extraction by Soxhlet method with eluotropic series for 8-12 hr¹⁶. The dry sample was dissolved in DMSO to form a 100 mg/ml stock & filtered by a 0.22 µm syringe filter for further use.

2.2 Qualitative Analysis of Phytoextracts

Qualitative analysis (alkaloids, fatty acids, cardiac glycosides, flavonoids, glycosides, phenols, resins, saponins, steroids, tannins, terpenoids) of *Bauhinia variegata* bark extracts was done using standard procedures¹⁷,¹⁸.

2.3 Determination of Antioxidant Activity by DPPH Assay

The antioxidant activity was measured using DPPH free radical assay by a standard protocol¹⁷.

2.4 In Vitro Culturing of Human Lung Cancer Cell Lines

Human lung cancer cell lines A549 and H460 were obtained from (NCCS, Pune, India). Cell lines were grown as per the standard protocol in controlled environment and supplements¹⁹.

2.5 MTT Method (Cytotoxic Assay)

The stock solutions of *Bauhinia variegata* bark extracts were prepared in 0.5 % Dimethyl Sulfoxide (DMSO) and diluted for further use (DMSO concentration

did not exceed 0.1 %). Cytotoxic potential of extract was determined by MTT assay¹⁹. Cells were grown in 96-well plates overnight and treated with different concentrations of bark extracts for 24 h, 48 h and 72 h time points. Untreated cells were taken as control. After 24, 48 and 72 h of incubation of cell lines with bark extracts, MTT assay was done using standard protocols¹⁹. The absorbance of each well was measured at 575 nm. IC50 value of extracts was calculated by determining percentage cell growth inhibition using Graph Pad Prism 6.0 software.

2.6 Soft Agar Colony Formation to Evaluate Cellular Transformation

For Colonogenic assay, the cells were plated in 6-well tissue culture plate with 5,000 viable cells (per well) as determined by the Trypan blue staining²⁰. A549 and H460 cells were allowed to grow overnight and after 24 h the fresh media modified with different concentrations of the different extracts were added for 48 h and 24 h respectively. The number of A549 and H460 cells after treatment with respective extracts were counted using a Neubauer Chamber. 2 % Agar was melted and cooled to 40°C in a water bath and media containing serum was added in equal volume to give 1 % base agar solution. 500µl of the base agar solution was pipetted into each well of a 24-well plate. 0.7 % agar was melted and cooled to 40 °C and mixed with media containing A549 cells treated with PEBE for 48 h.

For H460, 0.7 % agar was mixed with media containing H460 cells treated with CBE for 24 h. 500µl of this solution was pipetted onto the top agar. Cell number was maintained at 1250-1500 cells per well. The cells could grow for 13 -15 days for both cell line and in every 3-4 days, 200 µl of fresh media was added above the top layer as a feeder. After 15 days, the medium above the cells was removed and rinsed carefully with PBS. 2-3 ml of a mix of 6.0 % glutaraldehyde and 0.5 % crystal violet was added on cells and left for a minimum 20 min. The glutaraldehyde crystal violet mixture was removed and rinsed with water. The colony size was measured using Image J software.

2.7 Wound Healing Assay/Scratch Test

Cancer cells undergo epithelial to mesenchymal transition during metastasis^{21,22}. Cells were grown

and starved in low serum media (1.5 ml; 2 % serum in DMEM) overnight. A549 and H460 cells monolayers were scraped during a line to make a “scratch” with a pipette 200 µl tip. Cells were washed with PBS and low-serum media (2 % serum to prevent cell proliferation) was replaced with media containing different concentrations of extracts. A549 cells were treated with PEBE extract for 48 h and H460 cells with CBE for 24 h. Plates were placed in an incubator at 37 °C for 0-36 h. Cells were stained with crystal violet and images were captured at different time-points from 0 to 36 h respectively. The pictures acquired for every sample was further analyzed quantitatively by using computing software.

2.8 DNA Fragmentation Examination

A549 and H460 cells (5×10^6) were grown for 24 h and treated with various concentrations of PEBE and CBE for 48 h and 24 h, respectively. Cells were collected, washed with $1 \times$ PBS and centrifuged at 300 g. Cell pellet was collected and resuspended in 0.5 ml lysis buffer and incubated for 1.5 h at 37 °C followed by centrifugation at 10 K rpm for 15 min (at room temperature). Pellet was discarded and supernatant was mixed with equal volume of isopropanol followed by an addition of 25 µl of 4M NaCl and incubated at -20 °C overnight. Mixture was centrifuged again at 10 K rpm for 20 min and the pellet was dissolved in 40 µl ddH₂O. 5 µl of RNase A (10 mg/ml) was added to the lysate and further incubated for 1 h at 37 °C. The DNA was then electrophoresed in a 1.8% agarose gel in TAE (triacetate-EDTA) buffer (pH 8.0). After electrophoresis, ethidium bromide was used to stain the DNA and visualized using a gel-doc system (BIO-RAD).

2.9 Analysis of Intracellular Reactive Oxygen Species by DCHF-DA

The 2', 7'-dichlorodihydrofluorescein diacetate (H2DCF-DA) fluorescent probe is commonly employed that enabled the monitoring of intracellular accumulation of ROS. A549 and H460 cells were grown overnight in 6 well plates. Cells were treated with PEBE (A549) and CBE (H460) respectively and incubated for various time intervals (0 to 10h). At the end of the incubation period, the media was removed and 5 µM of DCHF-DA which is diluted in media was added to

the cells and incubated for 40 min at 37 °C. Remove the dye, trypsinize the cells and add media to stop its action. Centrifuge it at 1500 rpm for 3 min. The cells were then washed thrice with PBS and fluorescence intensity (excitation = 485 nm and emission = 530 nm) was measured by fluorimeter^{7,23}.

2.10 Fluorescent Microscopy Analysis by DAPI Staining and Acridine Orange/Ethidium Bromide Staining

Cell nuclear morphology was checked by fluorescence microscopy using DAPI²⁴ and AO/EtBr staining^{16,25}. A549 cells were treated with the PEBE for 48 h and H460 cells with CBE for 24 h followed by DAPI and AO/EB dye mix and examined under a Nikon Eclipse Ti fluorescence microscope.

2.11 Determination of Caspase-3 Activity in Cell Lines

Bio Vision Caspase-3 Colorimetric assay kit (K-106) was used to determine caspase-3 levels in A549 and H460 cell lines as per the protocol mentioned in the kit instruction manual.

2.12 TMRM Staining for Mitochondrial Membrane Potential Measurement

A549 and H460 cells were grown in 6-well plates and treated with PEBE (IC₅₀, 48 h) and CBE (IC₅₀, 24 h) respectively. The cells were stained with tetramethyl rhodamine, methyl ester and perchlorate (TMRM, 100 nM) at 37 °C for 30 minutes^{25,26}. After PBS wash, the cells were imaged using a fluorescence microscope.

2.13 Statistical Analysis

All experiments were done in triplicate, and data expressed as mean ± standard error of mean (SEM).

3. Results

3.1 Extract Preparation and Determination of Antioxidant Potential

Bauhinia variegata bark was ground after washing and drying, the powder so obtained was weighed and

subjected to solvent extraction by Soxhlet apparatus. Various fractions of crude extracts were collected and tested for their effects on A549 and H460 cell lines. The classes of phytochemicals present in these extracts were identified to be oils and fats, alkaloids, carbohydrates, saponin and glycosides in PEBE (while phenols, flavonoids and triterpenoids were absent and the CBE contained phytochemicals like (oils and fats, alkaloids, saponin, polyphenols, cardiac glycoside, tannin, and terpenoids (Data not shown here). GC-MS chromatogram of the PEBE of *Bauhinia variegata* clearly showed the presence of 18 compounds and GC-MS chromatogram of the CBE of *Bauhinia variegata* clearly showed the presence of 08 compounds (Data not shown here).

Further, the antioxidant potential of the extracts was determined by DPPH assay which showed that n-hexane and petroleum ether extracts showed lesser antioxidant activity as compared to other extracts. The methanolic and water extracts showed maximum antioxidant activity with the strongest DPPH radical scavenging activity among all the extracts (Figure 1). Percentage scavenging of DPPH free radical with different concentrations of *Bauhinia variegata* bark extracts here.

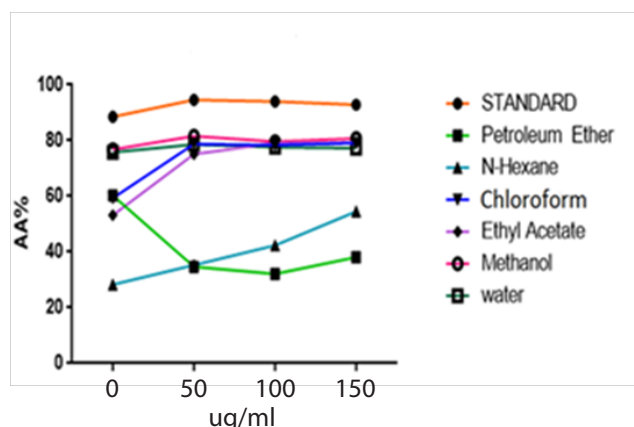


Figure 1. Percentage scavenging of DPPH free radical with different concentrations of *Bauhinia variegata* bark extracts.

3.2 MTT Assay: Potential for Cytotoxicity

3.2.1 Cytotoxic Screening of Extracts on A549 Cells by MTT Assay

The effect of the various extracts was evaluated on A549 cell line. Cytotoxic activities against A549 cells growth

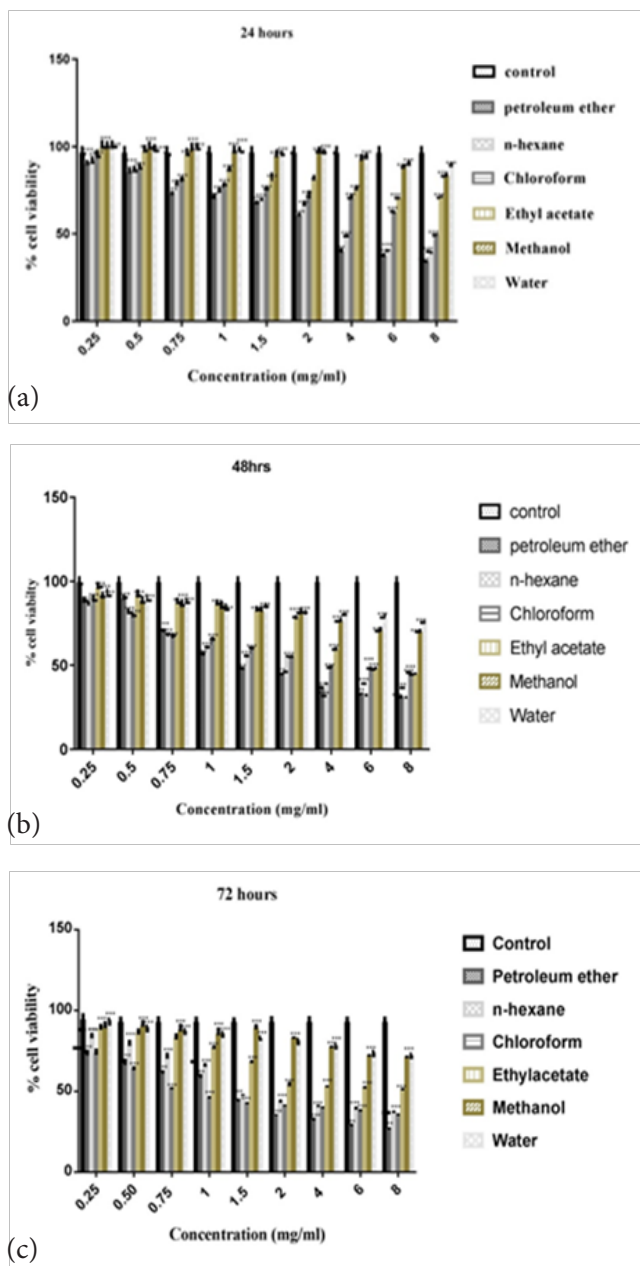


Figure 2. The effect of *Bauhinia variegata* bark extracts against A549 cell line for 24 h, 48 h and 72 h. Percentage growth proliferation of A549 cells was assayed at 100 mg/ml concentration of extracts using MTT assay as described in the Methods section (a) Effect of different concentrations of different bark extracts on A549 cells for 24 h (b) Effect of different concentrations of different bark extracts on A549 cells for 48 h (c) Effect of different concentrations of different bark extracts on A549 cells for 72 h respectively. Data represented as the mean \pm standard deviation of at least three experiments. *** $P < 0.001$.

were measured after treating with phytochemical extracts of PE, N-hexane, Chloroform, Ethyl acetate, Methanol and Water of *Bauhinia variegata* at concentrations of 0.25 mg/ml to 8mg/ml for 24 h, 48 h and 72 h. The results showed that A549 cells responded to the cytotoxic effects of the plant extracts in a dose and time-dependent manner.

Petroleum ether and n-Hexane extracts showed the foremost cytotoxic effect on A549 cell line as compared to other extracts at 48 h treatment. The polarities of Petroleum ether and n-hexane are almost similar and both the solvents have shown almost similar composition. Hence, it's likely that the cytotoxic agent (s) in both the solvents are identical. Therefore, Petroleum ether bark extract (PEBE) has been selected for the further study due to lesser yield of n-hexane extract. The cytotoxicity of PEBE on A549 cells increased from 33 % to 30 % to 26 % after 24, 48 and 72 h respectively. The cytotoxicity of PEBE on A549 cells is shown in Figure 2 a, b, c.

3.2.2 PEBE Inhibit Growth and Proliferation of A549 Cells

Examination of A549 cell morphology was done at 48 h treatment of PEBE and it was observed that from 0.5, 1, 1.5, 2 and 4 mg/ml concentrations cells had altered morphologically and started to shrink showing the symptoms of the cell death. The morphological examination of the cells after PEBE treatment showed cell shrinkage and rounding up of the cells which are typical features of cell death as shown in Figure 3.

3.2.3 Determination of IC₅₀ Value of PEBE Extract

Effect of different concentrations of PEBE of *Bauhinia variegata* on the viability of A549 cells for different time measure (at 24 h, 48 h and 72 h) was assessed. The IC₅₀ values were 2.8 mg/ml for 24 h, 1.6 mg/ml for 48 h and 1.5 mg/ml for 72 h as shown in Figure 4. The extract was more potent after 48 h treatment; hence this time point was selected for further experiments (Figure 4).

3.3 MTT Assay - H460 Cells

3.3.1 Cytotoxic Screening of Extracts on H460 Cells

The effect of the extracts on H460 cell line showed that the chloroform bark extract (CBE) had a greater

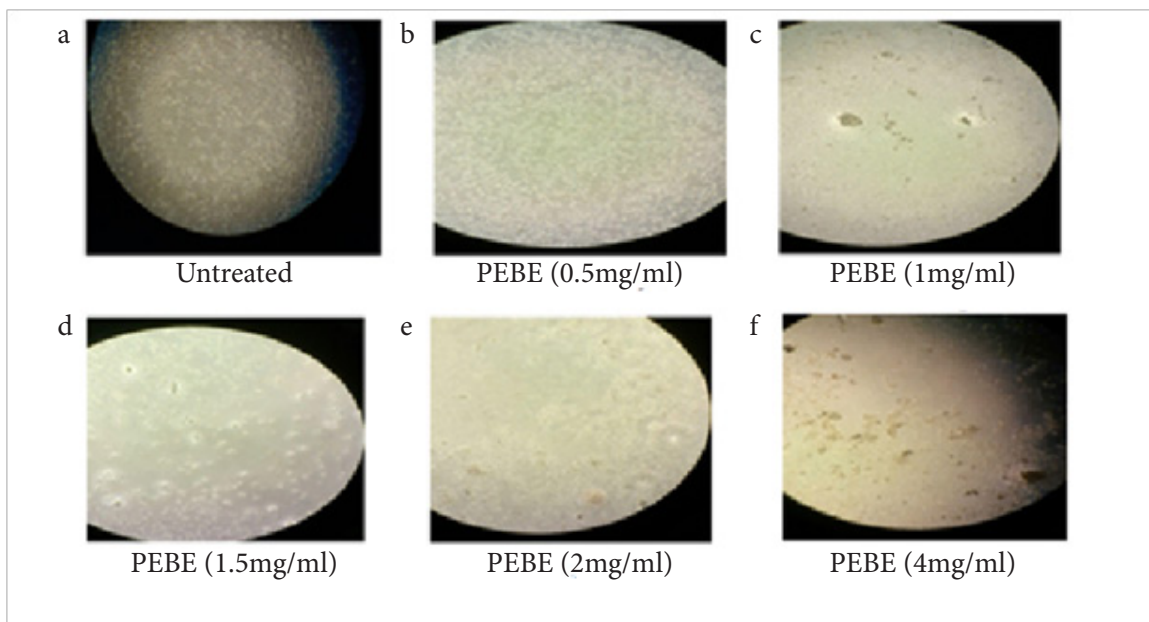


Figure 3. Morphological effects of A549 untreated cells (a) without treatment and cells exposed to (b) PEBE (0.5 mg/ml), (c) PEBE (1 mg/ml), (d) PEBE (1.5 mg/ml), (e) PEBE (2 mg/ml), (f) PEBE (4 mg/ml) of *Bauhinia variegata*.

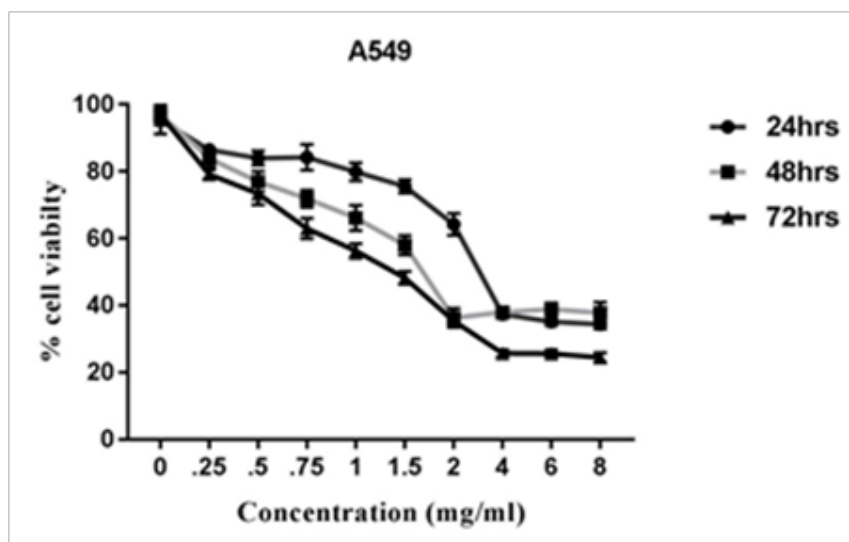
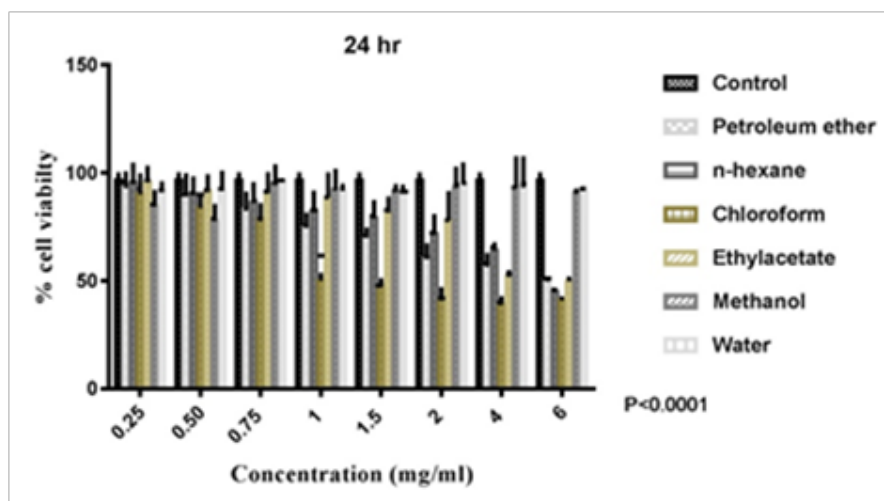
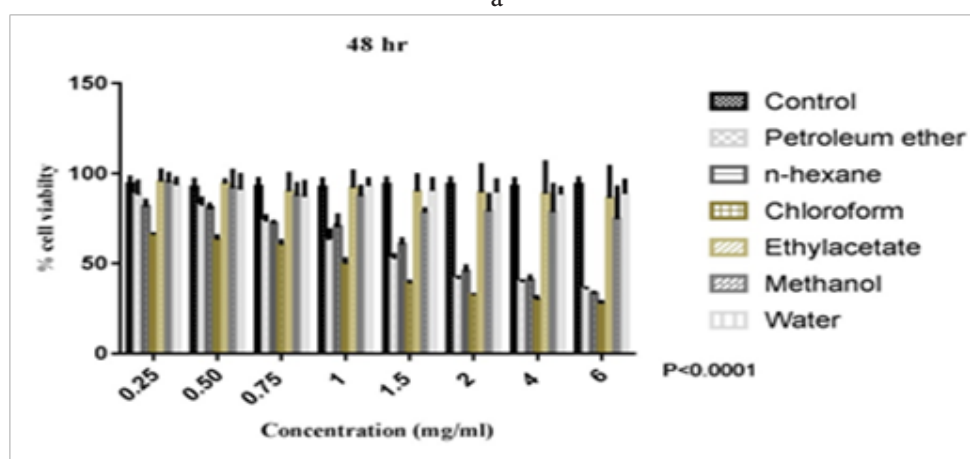


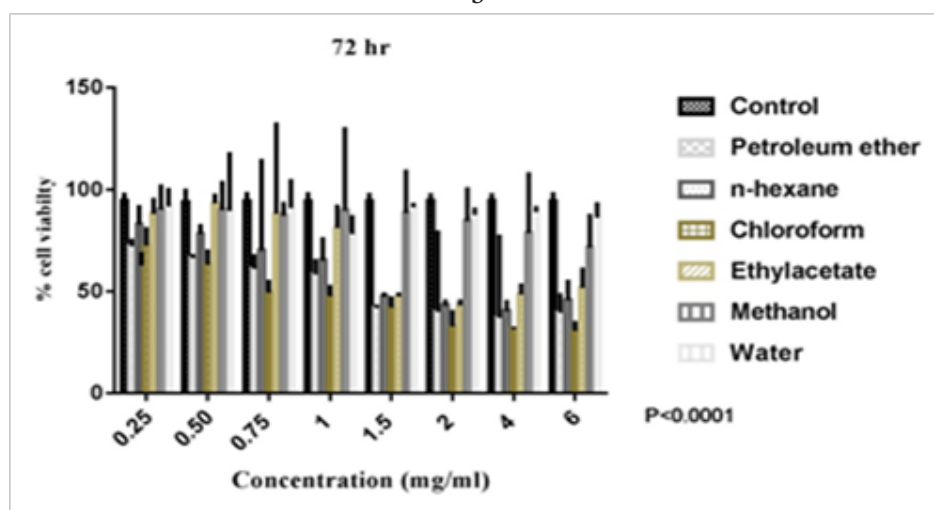
Figure 4. IC₅₀ values of crude petroleum ether bark extract of *Bauhinia variegata* on A549 cells for 24 h, 48 h, and 72 h (n=3).



a



b



c

Figure 5. The effect of *Bauhinia variegata* bark extracts against H460 cell line for 24 h, 48 h, and 72 h. Percentage growth proliferation of H460 cells was assayed at 100 mg/ml concentration of extracts using MTT assay as described in the Methods section — **a)** Effect of different concentrations of different bark extracts on H460 cells for 24 h **b)** Effect of different concentrations of different bark extracts on H460 cells for 48 h **c)** Effect of different concentrations of different bark extracts on H460 cells for 72 h respectively. Data represented as the mean \pm standard deviation of at least three experiments. ****P<0.0001.

cytotoxicity at 24 h treatment. The cytotoxicity of CBE on H460 cells was time dependent demonstrating a potent and definite growth inhibitory effect as shown in Figure 5. The cytotoxicity of CBE on H460 cells increased from 30.9 % to 27.9 % to 26 % after 24, 48 and 72 h respectively. The difference in the behavior of both cell lines may be due to their different molecular characteristics which are targeted by the different phytochemicals present in the two bark extracts (Figure 5 a, b, c).

3.3.2 CBE Inhibits Growth and Proliferation of H460 Cells

Examination of H460 cell morphology was done at 24 h treatment of CBE and it was observed that from 0.5, 1, 1.5, 2 mg/ml concentrations, cells had changed morphologically and started to shrink showing the symptoms of the cell death.

The morphological examination of the cells after CBE treatment showed as cell shrinkage and rounding up of the cells which are typical feature of cell death as shown in Figure 6.

3.3.3 Determination of IC50 Value of CBE Extract

Effect of different concentrations of CBE of *Bauhinia variegata* on the viability of H460 cells for different time interval (at 24 h, 48 h and 72 h) was assessed. The IC50 values were 1.0 mg/ml for 24 h, 0.78 mg/ml for 48 h and 0.74 mg/ml for 72 h as shown in Figure 7. The extract was more potent after 24 h than after 48 h treatment. The inhibitory concentrations for 24 and 48 h do not show much difference. So, the 24 h treatment was selected for further experiments on H460 cells (Figure 7).

3.4. Colony Growth Inhibition Studies - Soft Agar Assay

3.4.1 PEBE Inhibits A549 Colony Growth

The ability of PEBE to inhibit the expansion of tumors (cell colonies) and therefore the spread of cancer cells was assayed *in vitro*. PEBE significantly decreased A549 colony growth in a concentration-dependent manner showing significant antitumorigenic activity at 2 mg/ml as shown in Figure 8. The mean tumor diameter in the control (untreated) was 46.2 μm , while at 2 mg/

ml treatment the diameter was reduced to 30.4 μm as shown in Figure 8i. Quantitative analysis of these results is shown in Figure 8ii.

3.4.2 CBE Inhibits H460 Colony Growth

CBE significantly decreased colony growth of H460 cells in a concentration-dependent manner with a significant antitumorigenic activity at a concentration of 2 mg/ml Figure 9. The mean tumor diameter for control (untreated) is 63.38 μm which decreased to 27.93 μm in 2 mg/ml concentration treatment and showed a reduction in size of around 33.27 μm in diameter as shown in Figure 9i. Lower concentrations of 1 and 1.5 mg/ml showed no significant difference in mean tumor diameter as compared to control cells. Quantitative analysis of these results is shown in Figure 9ii.

3.5 Wound Healing Assay/ Scratch Test

3.5.1 PEBE Showed Slower Migration in A549 Treated Cells

Cell migration was investigated by performing the cell scratch assay. In A549 cells, as compared with the control group, gradual reduction was noticed within the number and rate of migrated cells with PEBE treatment. A slower rate of migration was observed with 0.5 and 1 mg/ml PEBE treatment while at 2 mg/ml the cells were unable to survive. Hence, this dose was excluded from the study. The distance was more between the edges of the wound when A549 cells were treated with PEBE for 12 to 36 h, demonstrating the reduced migration of A549 cells as shown in Figure 10i. Quantitative analysis of the scratch diameter is shown in Figure 10ii.

3.5.2 CBE Showed Slower Migration in H460 Treated cells

The effect of different concentrations of CBE extract on H460 cells after 24 h treatment indicated a dose-dependent decrease in viability of cells in comparison to control cells. H460 cells also showed slower migration and wound healing with 1 mg/ml and 1.5 mg/ml CBE treatment. CBE impaired cell migration for 12 to 30 h as shown in. The cells lost their viability at 2 mg/ml treatment, and hence this dose was not included for

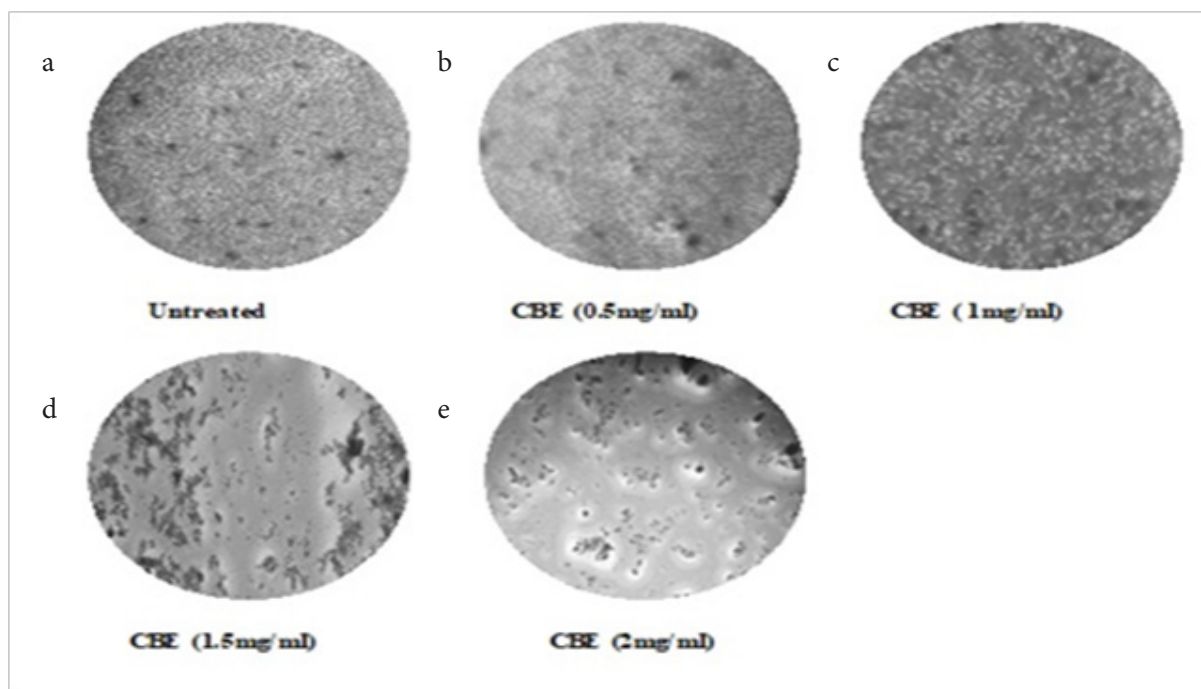


Figure 6. Morphological effects of H460 untreated cells **a)** without treatment, and cells exposed to **b)** CBE (0.5 mg/ml), **c)** CBE (1 mg/ml), **d)** CBE (1.5 mg/ml), **e)** CBE (2 mg/ml) of *Bauhinia variegata*.

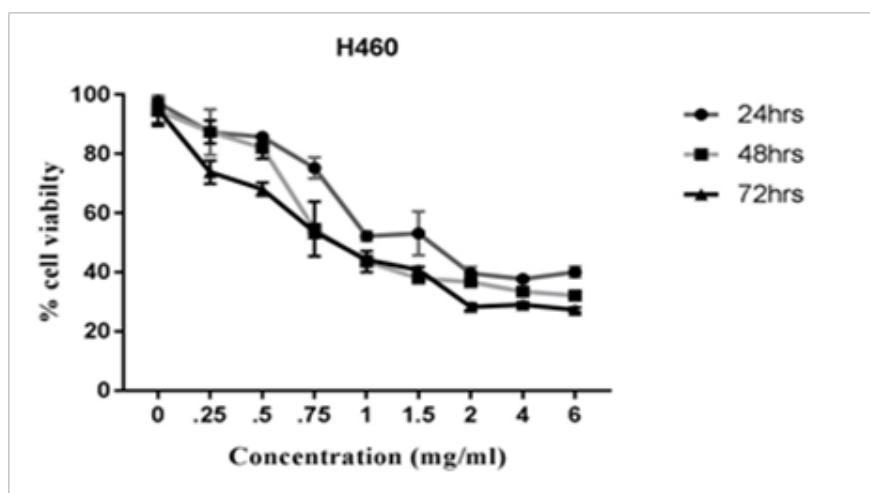


Figure 7. IC50 values of crude chloroform bark extract of *Bauhinia variegata* on H460 cells for 24 h, 48 h, and 72h (n=3).

the comparison as shown in Figure 11i. Quantitative analysis of the scratch diameter is shown in Figure 11 ii.

3.6 DNA Fragmentation Studies

3.6.1 PEBE Induces Cellular DNA Fragmentation in A549 Cells

In order to explain the mechanism of cell apoptosis mediated by PEBE, we performed a DNA fragmentation assay, since DNA fragmentation is the characteristic

for apoptosis. Treatment of cells with different concentrations of PEBE for 48 h, led to a decrease in band intensity of DNA with increasing concentration of PEBE in 1 % agarose gel electrophoresis as shown in Figure 12a. A typical DNA ladder pattern of internucleosomal fragmentation was observed with after 48 h of treatment as shown in Figure 12b. The late stages of apoptosis are characterized by damage (fragmentation) of DNA²⁷. These data suggest that PEBE extract is an effective inducer of Apoptosis.

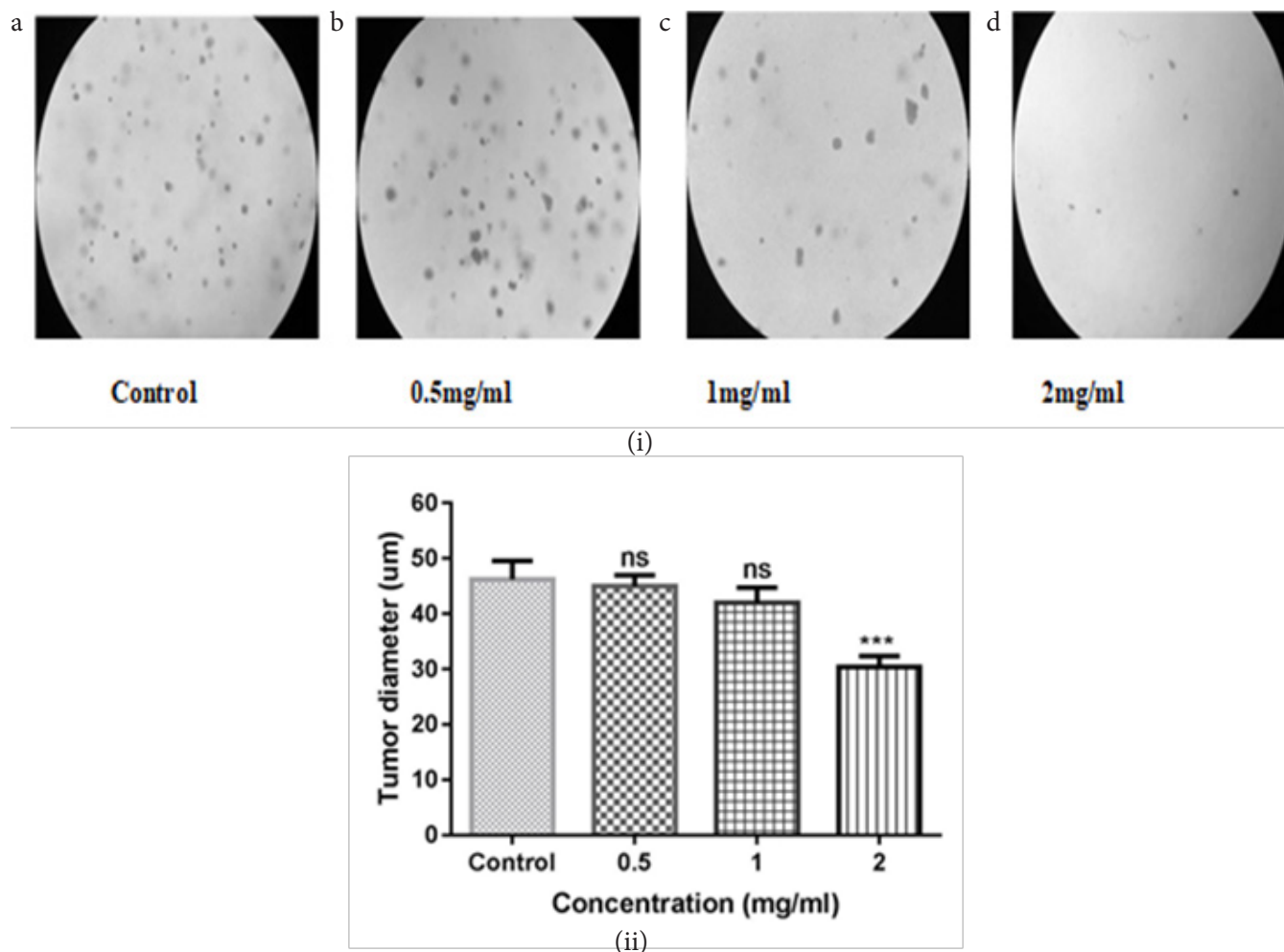


Figure 8. Representative images for *in vitro* assay to assess the anti-tumorigenic activity of the PEBE on A549 cells. Cell colonies in soft agar in (i) a) Untreated cells, b) 0.5 mg/ml PEBE treatment, c) 1 mg/ml PEBE treatment, d) 2 mg/ml PEBE treatment; $n = 3$. Quantitative analysis of mean tumor (colony) diameter of different concentrations of PEBE is shown in (ii) Values are the means \pm SD of at least three independent experiments; *** $P < 0.001$, ns = non-significant.

3.6.2 CBE Induces Cellular DNA Fragmentation in H460 Cells

Fragmentation of genomic DNA (light fragments) was observed in H460 cell line treated with 2 and 4 mg/ml of CBE for 24 h as shown in Figure 13. A typical ladder pattern of internucleosomal fragmentation was observed in H460 cell line after 24 h at higher concentrations of CBE. Low-molecular-weight DNA from these cells was resolved in 2.0 % agarose gels. These data suggest that CBE is a potent inducer of apoptosis. Further studies are needed to establish the role of the interaction of CBE with DNA in cancer cells.

3.7 Quantification of ROS

3.7.1 Effects of PEBE on Intracellular ROS Levels of A549 Cells- DCHF-DA Assay

ROS levels were examined at indicated time points (0 to 10 h) after PEBE treatment on A549 cells and it was seen that the ROS levels reached a maximum at about 6 h (29.5 %, as compared to 8 % at 0 h), but subsequently decreased as shown in Figure 14. On treatment with PEBE, intracellular ROS elevates at initial hours and decrease subsequently which suggest they could be activating downstream signaling pathway resulting in apoptosis. These results indicate that ROS production is an early phase event in apoptosis induced by PEBE.

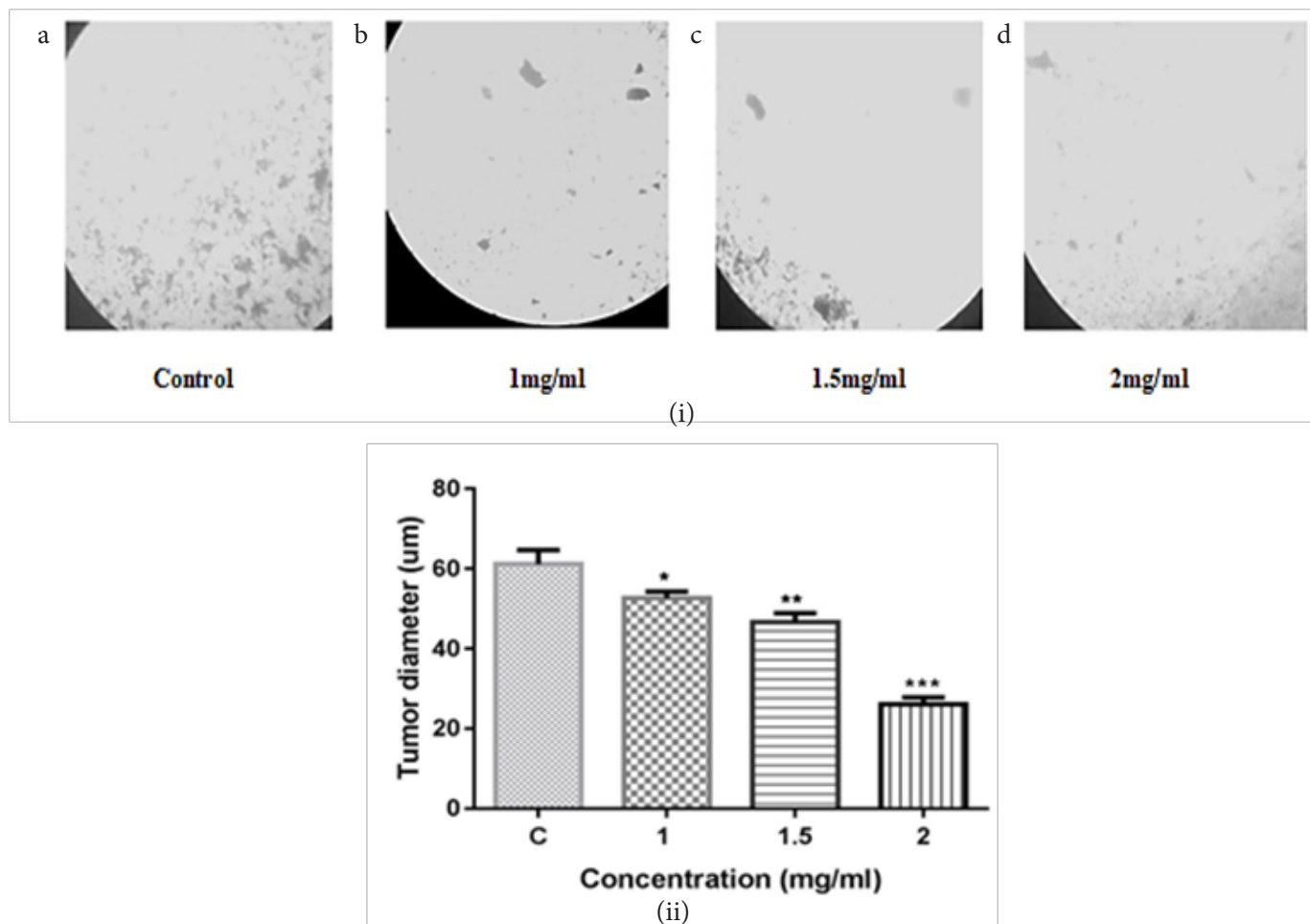


Figure 9. Representative images for the *in vitro* assay to assess the anti-tumorigenic activity of the CBE on H460 cells. Cell colonies in soft agar in (i) a) Untreated cells, b) 1mg/ml CBE treatment, c) 1.5 mg/ml CBE treatment, d) 2mg/ml CBE treatment; n = 3. Quantitative analysis of mean tumor (colony) diameter of different concentrations of CBE is shown in (ii) Values are the means \pm SD of at least three independent experiment: **P<0.01., ***P<0.001.

3.7.2 Effects of CBE on Intracellular ROS Levels of H460 Cells - DCHF-DA Assay

Recent studies have shown that ROS levels in a cell may have a significant role to play in the outcome of therapeutic agents²⁸. After exposure of H460 cells to CBE, ROS levels first increase then there is a little decrease at 6h and then stability increase within the cells as shown in Figure 15. Data showed that CBE increased ROS generation from 2 to 10h treatment.

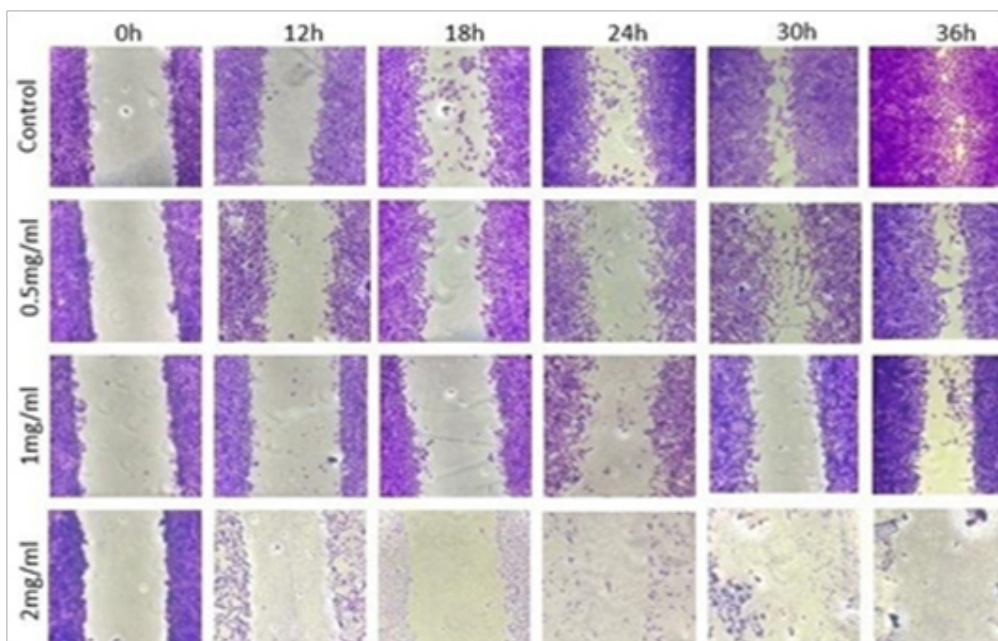
3.8 Alterations in Nuclear Morphology - DAPI Staining

DAPI staining was done after treatment of A549 cells with PEBE (1 mg/ml) showed chromatin condensation, nuclear fragmentation (“horse-shoe” like appearance

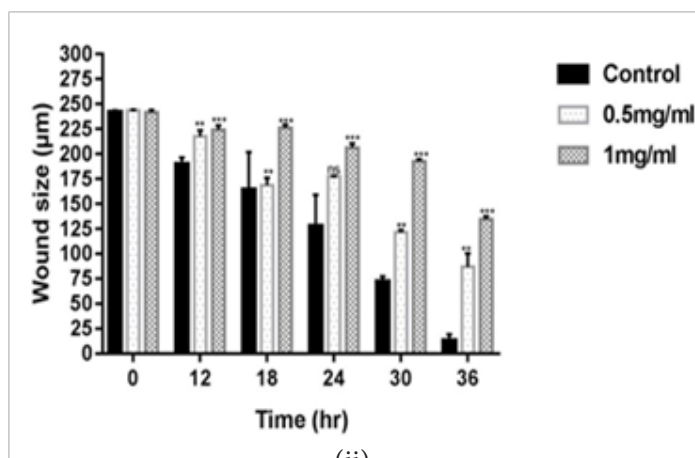
of nucleus) and cell shrinkage with an increase in apoptotic bodies in cells treated with 1.5 mg/ml PEBE for 48 h as shown in Figure 16 a, b, c. The control cells had round homogenous nuclei. The morphological changes associated with apoptosis such as margination of nucleus, chromatin condensation and nuclear fragmentation marked by arrows in Figure 16 d, e, f in H460 cells after 24h treatment with increasing concentrations (IC₅₀) of extracts is very distinct.

3.9 AO/EtBr Staining

Live cells with normal morphology were abundant in the A549 control group whereas early apoptotic cells were observed on treatment with 1 mg/ml PEBE concentration. Both early and late apoptotic cells were

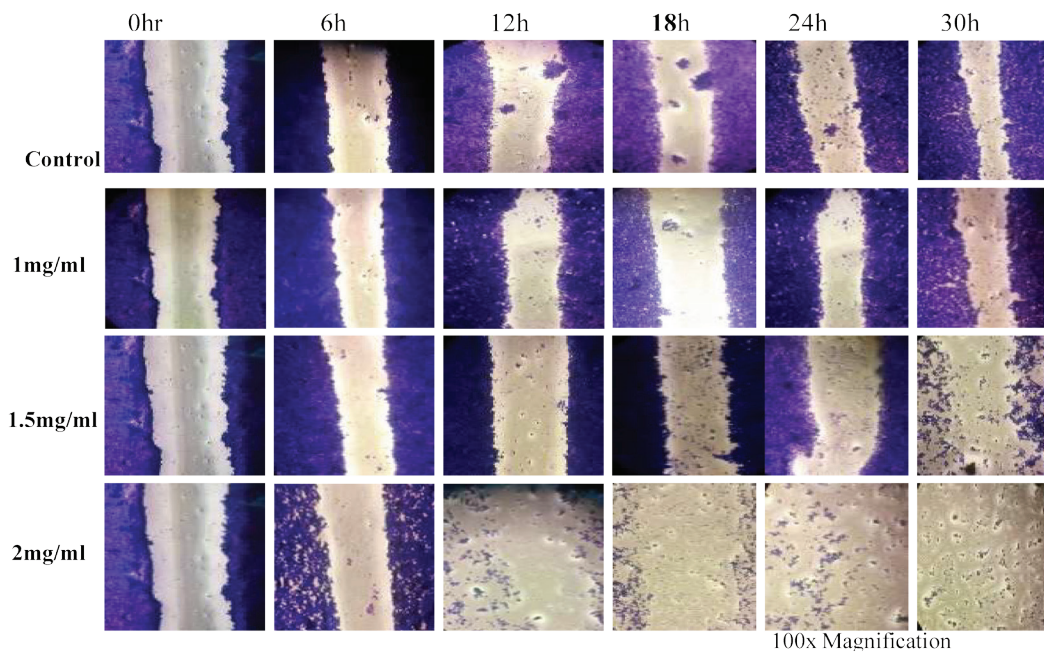


(i)

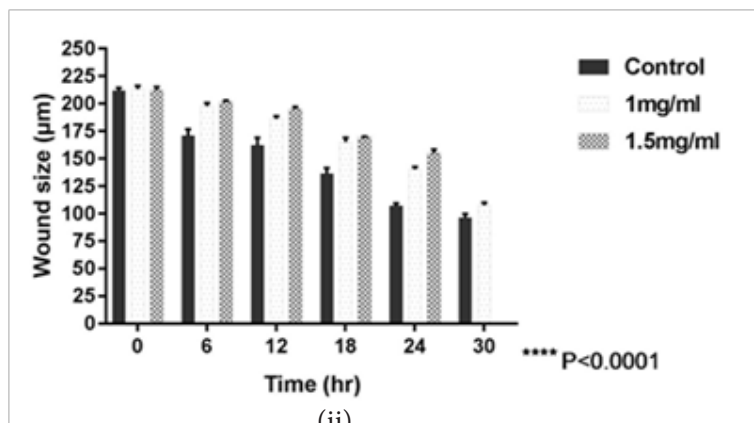


(ii)

Figure 10. Representative images are the results of *in vitro* scratch test to assess effect of PEBE on cell migration of A549 cells; $n = 3$. PEBE inhibits migration of A549 cells as shown in (i). Wound healing assay to determine the effect of PEBE on A549 cell migration at 0.5, 1, 1.5 and 2mg/ml concentrations for 36h. Quantitative analysis of wound size (μm) within 36 h. is represented in (ii). Error bars indicates the standard error of the mean of three independent experiments. $**P < 0.01$, $***P < 0.001$.



(i)



(ii)

Figure 11. Representative images for the results of *in vitro* scratch test to assess effect of CBE on cell migration; n = 3. CBE inhibits migration of H460cells (i) Wound healing assay to determine the effect of CBE on H460 cell migration. Quantitative analysis of wound size (µm) within 30 h, is measured here in (ii) Error bars indicate the standard error of the mean of three independent experiments: ***P<0.001.

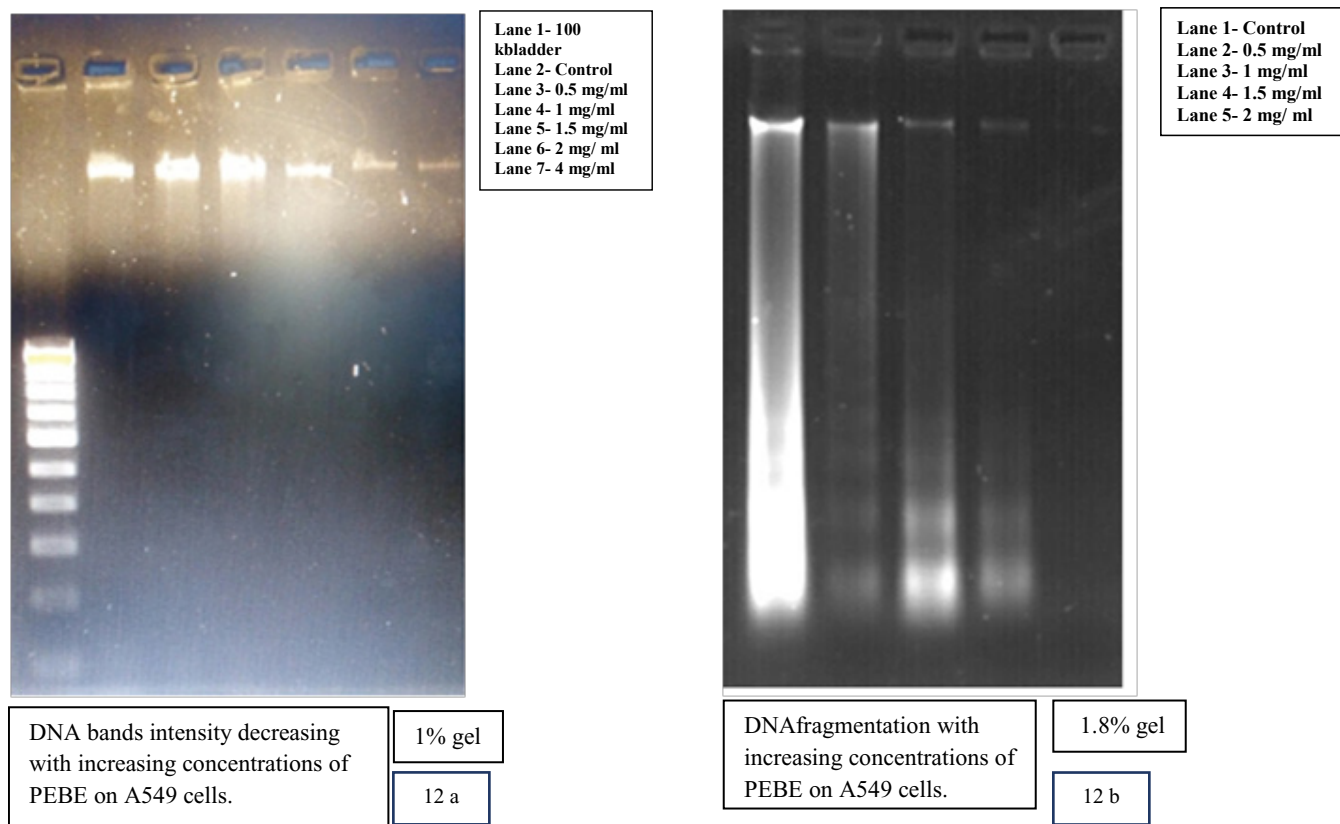


Figure 12. Representative images of DNA laddering in A549 cells **(a)** Cells treated with different concentrations of PEBE for 48 h results in decrease in DNA bands with increasing concentration of PEBE in 1% agarose gel electrophoresis, **(b)** Cells treated with increasing concentrations of PEBE for 48 h, and results in typical laddering pattern in 1.8% agarose gel electrophoresis.

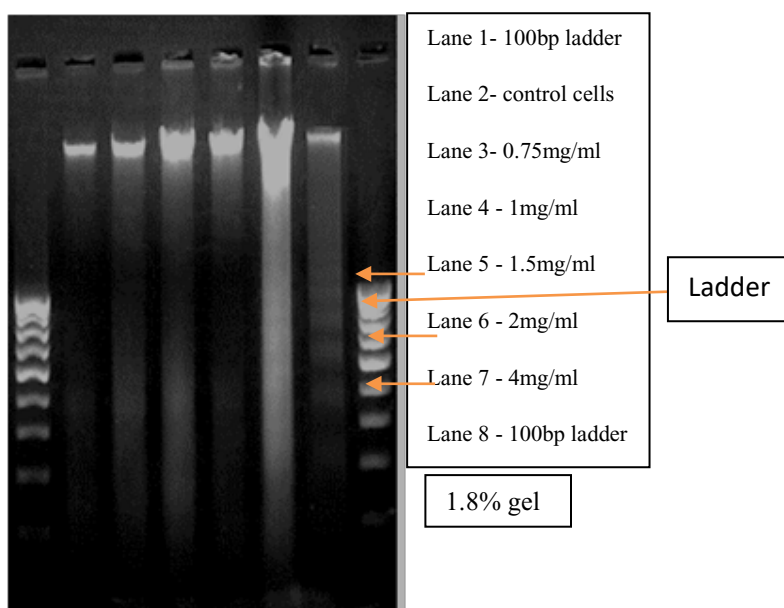


Figure 13. Representative images of DNA laddering in H460 cells. Cells treated with increasing concentrations of CBE for 24 h and results in typical laddering pattern in 1.8% agarose gel electrophoresis.

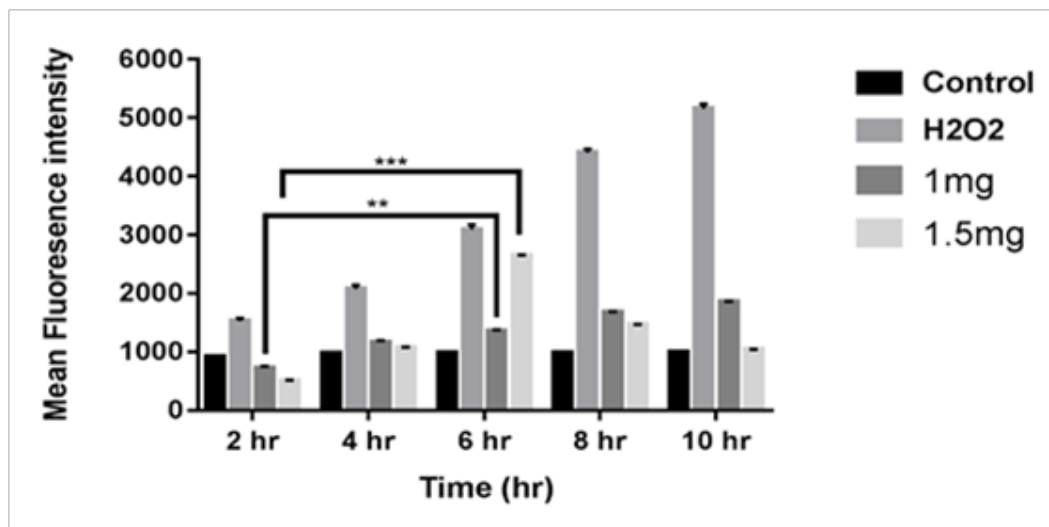


Figure 14. Time - dependent changes in ROS levels of A549 cells at different concentrations of PEBE. Data expressed as mean \pm SEM, ** $p < 0.01$, *** $p < 0.001$ as compared to control.

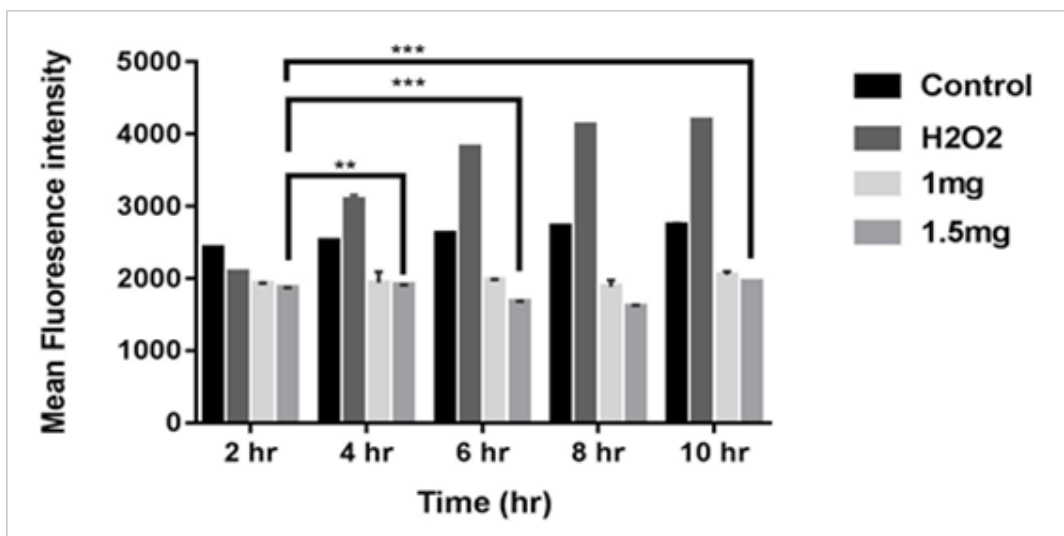
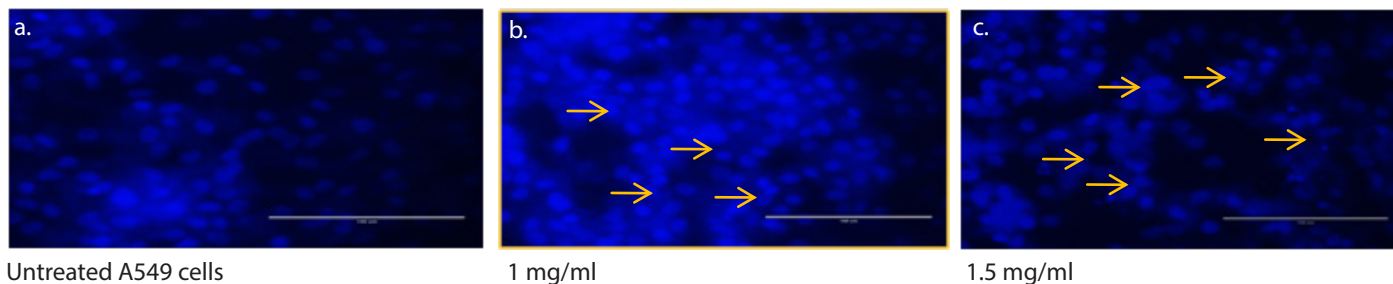
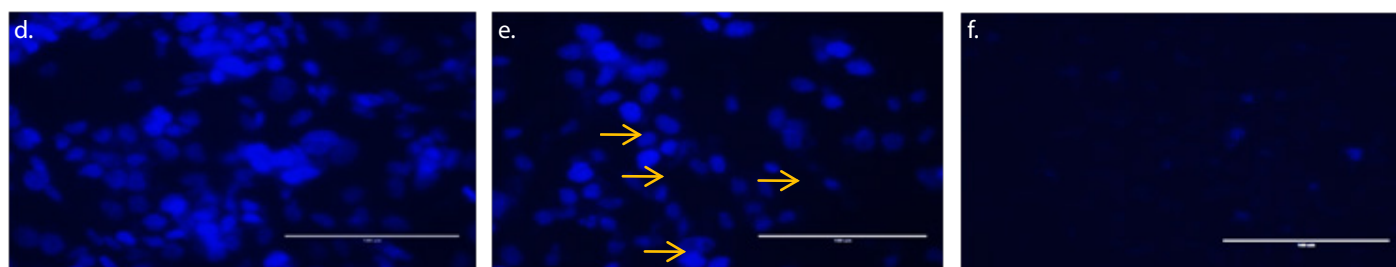


Figure 15. Time - dependent changes in ROS levels of H460 cells at different concentrations of CBE. Data expressed as mean \pm SEM, ** $p < 0.01$, *** $p < 0.001$ as compared to control.



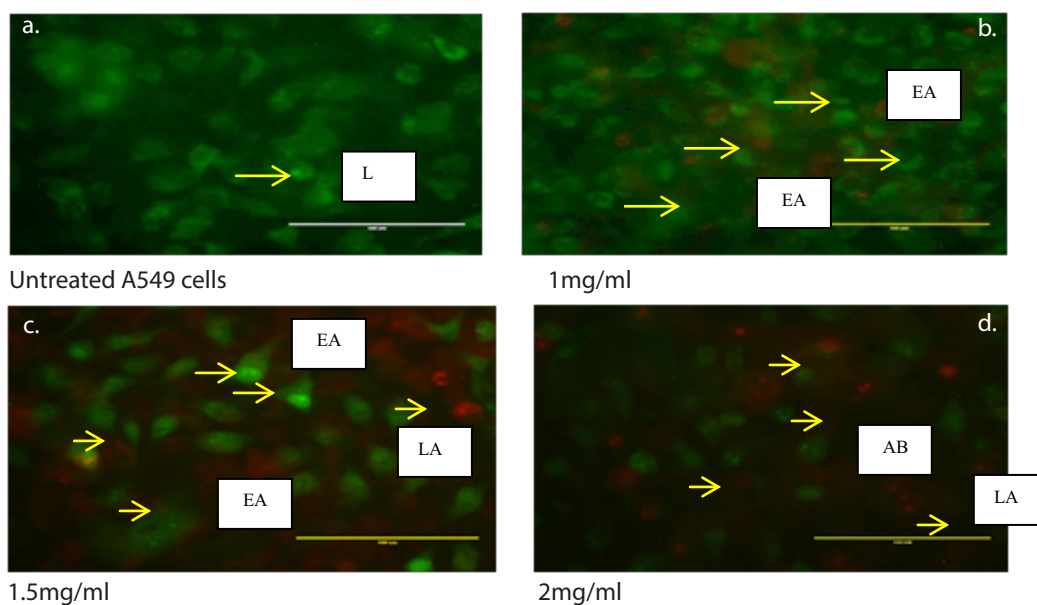


Untreated H460 cells

1 mg/ml

1.5 mg/ml

Figure 16. The effect of PEBE on apoptotic potential in A549 cells was evaluated using DAPI staining. **a)** control group; **b)** in the presence of 1 mg/ml; **c)** 1.5mg/ml of PEBE of *Bauhinia variegata* for 48 h under fluorescence microscope, Scale bar-100 um, Mag- 40x. Effect of CBE on apoptotic potential in H460 cells was evaluated using DAPI staining **d)** control H460 cells **e)** 1 mg/ml **f)** 1.5 mg/ml CBE of *Bauhinia variegata* for 24 h under fluorescence microscope, Scale bar-100 um, Mag- 40x. Arrow indicates chromatin condensation, nuclear fragmentation, horse- shoe shape nuclei and cell shrinkage in treated cells as compared to control cells.



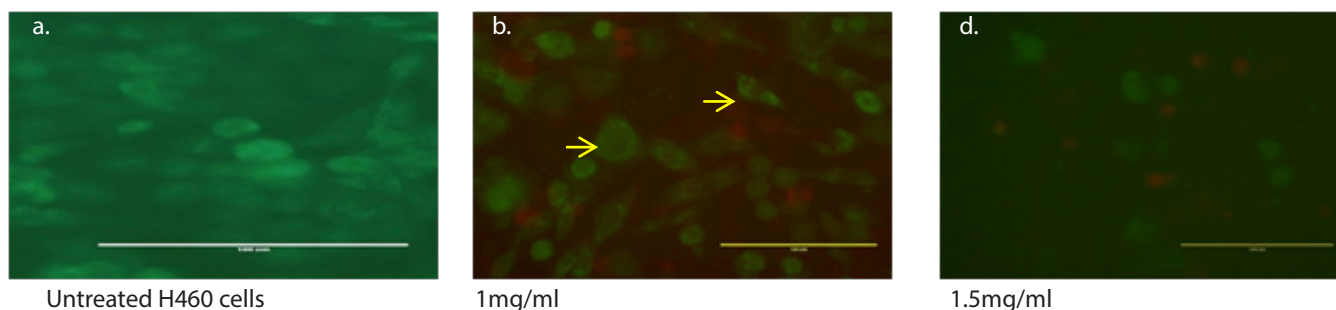
Untreated A549 cells

1mg/ml

1.5mg/ml

2mg/ml

Figure 17. A549 cells were stained by AO/EB and observed under fluorescence microscope: **a)** A549 control group; **b)** in the presence of 1 mg/ml; **c)** 1.5mg/ml; **d)** 2mg/ml of PEBE for 48h. Control wells were treated with equivalent amount of medium alone. Green live cells showed normal morphology with uniform nuclei; yellow early apoptotic cells showed nuclear margination and chromatin condensation. Late orange/red apoptotic cells showed fragmented chromatin and apoptotic bodies.



Untreated H460 cells

1mg/ml

1.5mg/ml

Figure 18. H460 cells were also stained by AO/EB and observed under fluorescence microscope: **a)** control group; **b)** in the presence of 1 mg/ml; **c)** 1.5mg/ml of CBE for 24h. Green live cells showed normal morphology with uniform nuclei; yellow early apoptotic cells showed nuclear margination and chromatin condensation. Late orange/red apoptotic cells showed fragmented chromatin and apoptotic bodies.

observed in A549 cell line treated with 1, 1.5 and 2 mg/ml concentrations. The 2 mg/ml treatment showed the greatest number of apoptotic bodies, and the cells were mostly in the late apoptotic stage as shown by arrows in Figure 17 a, b, c, d. Live cells appeared green, while early apoptotic appeared bright green or yellow and late apoptotic appeared red with condensed and fragmented nuclei.

For H460 cell line, live cells with normal morphology were abundant in H460 control group. H460 cell line treated with 1 mg/ml CBE showed early apoptotic cells while H460 cell line treated with 1.5 mg/ml CBE

showed late apoptotic bodies as shown in Figure 18 a, b, c.

3.10 Caspase-3 Activity in Cell Lines after PEBE and CBE Treatment

Caspase-3, a marker of apoptosis and has shown to be adequate for potent activation of apoptosis^{29,30}. Caspase 3 activity significantly increased in PEBE treated A549 cells and CBE treated H460 cells at the IC₅₀ value after 24 h to 48 h treatment. After 48 h of incubation of A549 cell line with PEBE there was a 3-fold increase in

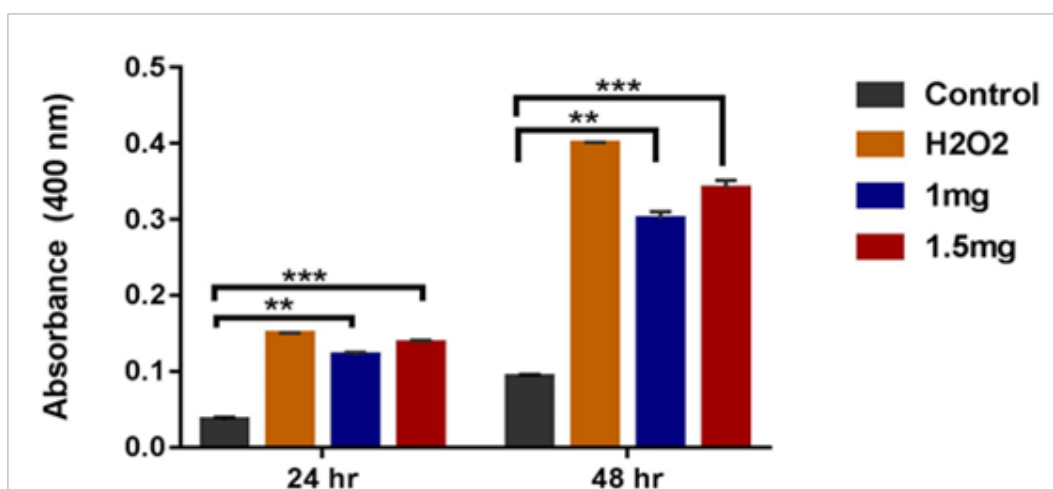


Figure 19. A549 cells were seeded in 24 well plates, then treated with PEBE in concentration and time - dependent manner. Caspase-3 activity were measured spectrophotometrically by detection of chromophore pNA at 405nm. Data expressed as mean \pm SEM, n=3 **p < 0.01, ***p < 0.001 as compared to control.

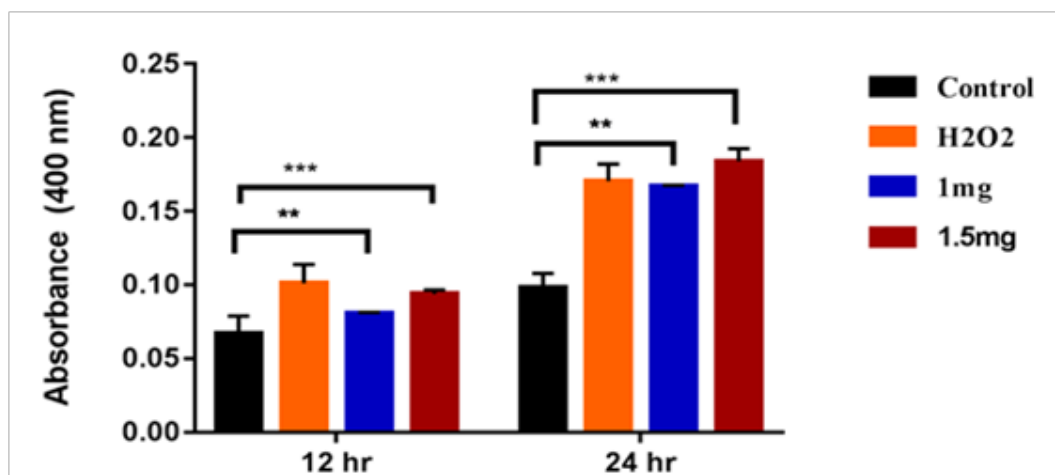


Figure 20. H460 cells were seeded in 24 well plates, then treated with CBE in concentration and time - dependent manner. Caspase-3 activity were measured spectrophotometrically by detection of chromophore pNA at 405nm. Data expressed as mean \pm SEM, n=3 **p < 0.01, ***p < 0.001 as compared to control.

caspase-3 levels as compared to A549 control cells as shown in Figure 19.

Caspase-3 activity significantly increased at IC₅₀ value of CBE from 12 h to 24 h treatment in H460 cell line as shown in Figure 20. From these data, we can say that Caspase-3 may also function before or at the stage when commitment to loss of cell viability is made.

3.11 Alteration in Mitochondrial Membrane Potential by TMRM Staining

Cell health can be assessed by proper functioning of mitochondria which can be monitored by observing changes in mitochondrial membrane potential (MMP). The role of intrinsic apoptosis pathway was further

validated by the changes in mitochondrial membrane potential in A549 cells treated with PEBE (1 mg, 1.5 mg) for 48 h and H460 cells treated with CBE at (1 mg, 1.5 mg) for 24 h. PEBE and CBE significantly decreased the mitochondrial membrane potential ($\Delta\Psi_m$) in A549 as shown in Figure 21 a, b, c and H460 cells as shown in Figure 21 d, e, f with increasing concentrations.

4. Discussion

Our data validates with proof of mechanism demonstrating the efficacy of *Bauhinia variegata* PEBE against A549 cells proliferation and CBE against H460 cells thus targeting two types of lung cancer cell lines widely used for such studies^{31,32}. We demonstrate potent antiproliferative activity with very low antioxidant

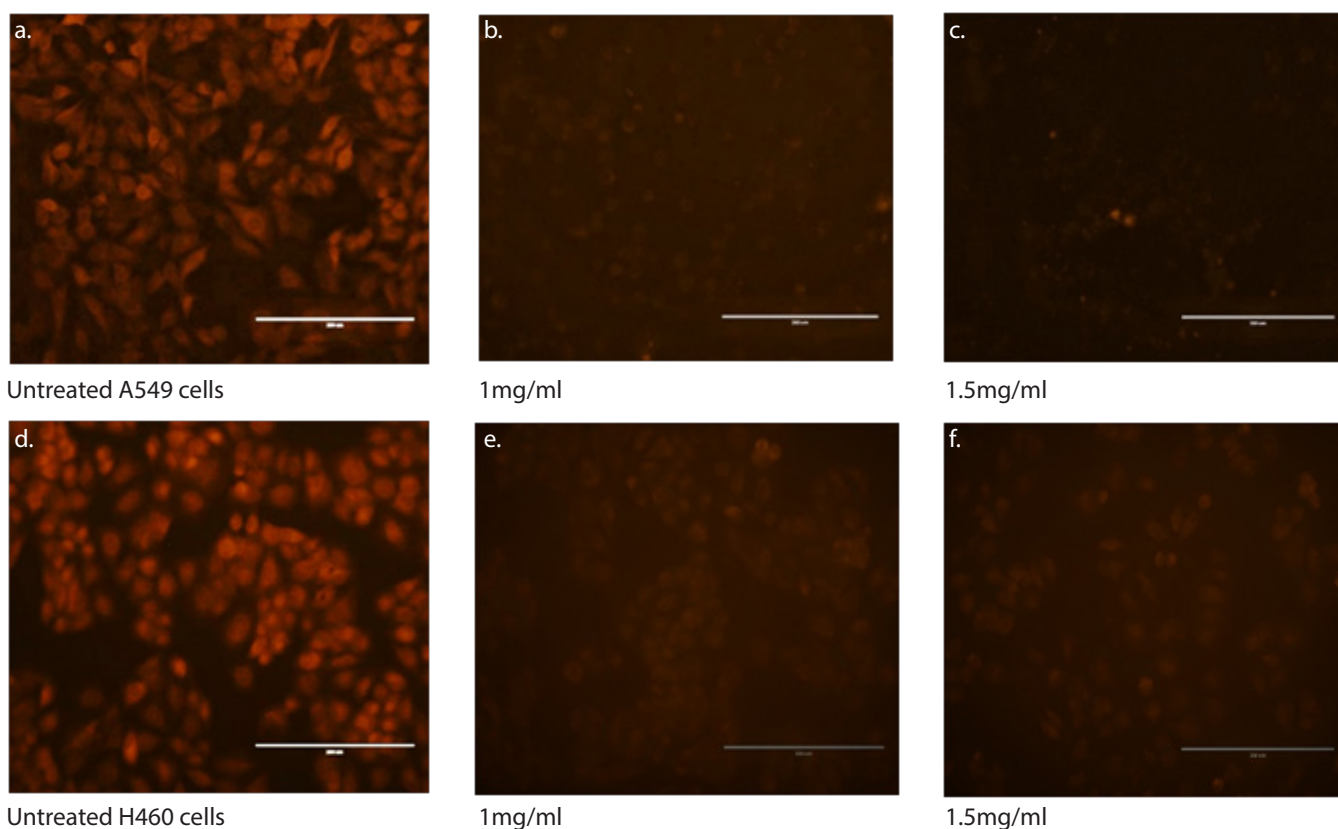


Figure 21. Cells were stained with TMRM and imaged by standard fluorescence techniques. PEBE (1 mg/ml, 1.5 mg/ml) for 48 h did not show significant change in TMRM fluorescence intensity in A549 cells (**a - c**), while CBE (1 mg/ml, 1.5 mg/ml) for 24 h significantly decreased TMRM fluorescence intensity in H460 cells (**d - f**).

capacity indicating its function via modulation of cellular redox status.

All of the *Bauhinia variegata* bark extracts were differently inhibiting A549 cells proliferation but petroleum ether extract was found to be the foremost potent inhibitor of A549 cells proliferation at 48 h treatment which was estimated by MTT assay (Figure 2) with IC₅₀ of 1.5 mg/ml at 48 h treatment (Figure 4). The IC₅₀ value of PEBE was determined and guided the treatment design. The ability of PEBE to inhibit the expansion of tumors (cell colonies) and therefore the spread of cancer cells was assayed *in vitro*. We next assessed the effect of PEBE treatment on Clonogenic survival of the A549 cells. Clonogenic study revealed that PEBE showed significant anti-tumorigenic activity as shown in (Figure 8) and (Figure 10) showed a depreciation in the wound closure ability of A549 cells after treatment in time and dose dependent manner as compared to the control cells. The study also tried to probe into the molecular mechanism behind the cytotoxic effect of PEBE. Cytoarchitectural changes due to DNA fragmentation is one of the hallmarks of apoptotic pathway. Treatment with PEBE showed a decrease in DNA bands (Figure 12a) and fragmentation of genomic DNA was observed at 48 h treatment (Figure 12b). Increase in ROS levels in cancer cells may contribute to the biochemical and molecular changes necessary for tumor initiation, promotion, progression,

and chemoresistance. The pattern of changes in ROS level was monitored (Figure 14) as it has a bearing on the drug sensitivity of the cell towards anticancer compounds. This result indicates that ROS production is an early phase in apoptosis induced by PEBE treatment. The morphological changes were detected by DAPI staining (Figure 16 a, b, c) and AO/EtBr staining as shown in (Figure 17 a, b, c, d). Caspase-3, an important effector of apoptosis got activated by PEBE treatment on A549 cells after 48 h (Figure 19). The decrease in MMP of A549 cells treated with various concentrations of PEBE was observed using TMRM dye (Figure 21a, b, c as compared to control cells showing the occurrence of apoptosis.

Comparative studies were also carried out in H460 cells (large cell carcinoma). All of the *Bauhinia variegata* bark extracts were differently inhibiting H460 cells proliferation but chloroform bark extract was found to be the foremost potent inhibitor of H460 cells proliferation followed by petroleum ether bark extract as shown in (Figure 5) with IC₅₀ of 1 mg/ml at 24 h (Figure 7). Clonogenic ability of CBE shows significant difference in mean tumor diameter as shown in (Figure 9) and slower migration and wound healing was observed in (Figure 11) as compared to H460 control cells. CBE acted *via* the apoptotic pathway & showed fragmentation of genomic DNA in dose and time dependent manner (Figure 13). Increase in ROS was

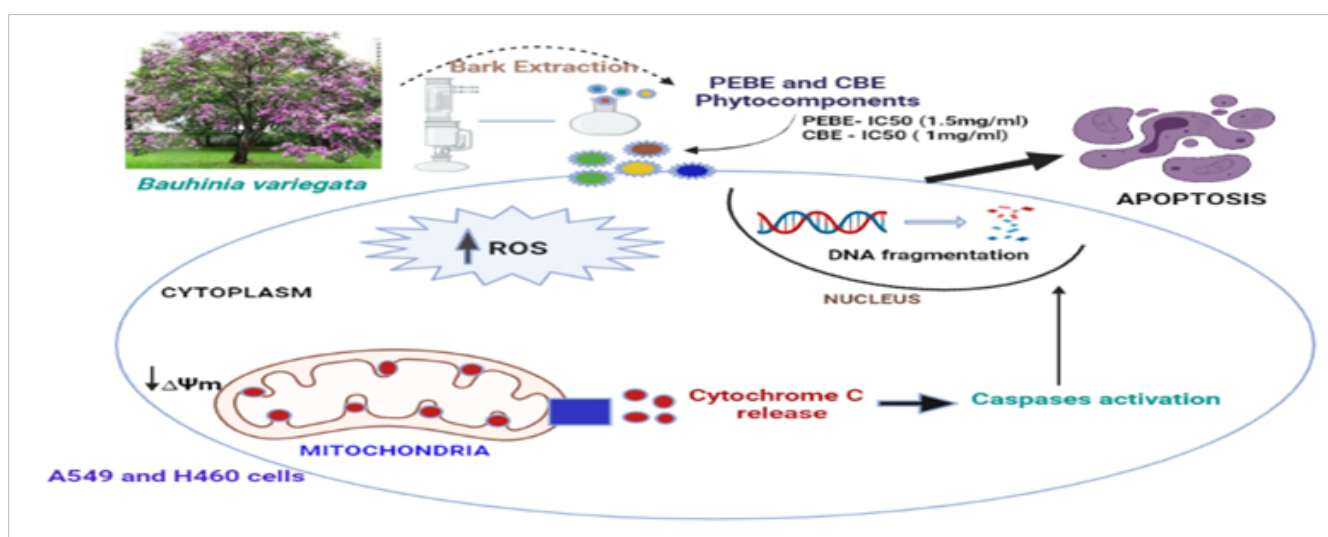


Figure 22. Proposed signaling pathways activated by Petroleum ether and Chloroform bark extracts of *Bauhinia variegata* leading to the observed anticancer effect.

responsible for CBE-induced apoptosis in H460 cell line (Figure 15). Morphological changes in apoptotic cells were detected by DAPI staining (Figure 16 d, e, f) and AO/EtBr staining as shown in (Figure 18 a, b, c). Unraveling the molecular mechanism showed that CBE causes the activation of caspase-3 in H460 cells at 24 h treatment. Further, there is a decrease in MMP of H460 cells treated with various concentrations of CBE as compared to untreated cells, which was observed using TMRM dye.

PEBE and CBE induced apoptosis of A549 and H460 cell lines may be through the activation of caspase-3 signaling and mitochondrial cell death mediated pathway, leading to the observed anti cancerous effect as shown in Figure 22. Our data suggest that PEBE and CBE possess strong antiproliferative effects against lung cancer cells with low toxicity. Plants are such a repertoire of molecules with phenomenal properties waiting to be unraveled. Study like this may seem like a drop in the ocean but they are necessary in retaining a hope for an alternative drug for the cancer treatment.

5. Conclusion

Thus, it can be concluded that phytochemicals from *Bauhinia variegata* hindered a normal growth of A549 and H460 cancer cell lines by inducing apoptosis, inhibiting colony formation, decreasing cell migration, increasing intracellular ROS levels, activating Caspases and decreasing Mitochondrial matrix potential. We have narrowed down on few phytochemicals by GC-MS analysis and one of this could be a strong contender for treatment of this disease.

6. Acknowledgement

TK did most of the experiments, AD helped in data analysis, JV and DJ helped with some experiments, SP helped in establishing the cell culture facility, PR conceptualized the project. We thank the Forest Officer, Waghai Botanical Garden, for permission to collect samples. The project was supported by research grant to PR and fellowship to TK by Gujarat State Biotechnology Mission, Gandhinagar, India.

7. References

1. Parikh PM, Ranade AA, Govind B, Ghadyalpatil N, Singh R, Bharath R, *et al.* Lung cancer in India: Current status and promising strategies. *South Asian J Cancer.* 2016; 5(03):093-5. <https://doi.org/10.4103/2278-330X.187563>. PMID:27606289. PMCID:PMC4991145
2. Zappa C, Mousa SA. Non-small cell lung cancer: Current treatment and future advances. *Transl Lung Cancer Res.* 2016; 5(3):288. <https://doi.org/10.21037/tlcr.2016.06.07>. PMID:27413711. PMCID:PMC4931124
3. Lu T, Yang X, Huang Y, Zhao M, Li M, Ma K, *et al.* Trends in the incidence, treatment, and survival of patients with lung cancer in the last four decades. *Cancer Manag Res.* 2019; 11:943. <https://doi.org/10.2147/CMAR.S187317>. PMID:30718965. PMCID:PMC6345192
4. Debevec L, Debeljak A. Multidisciplinary management of lung cancer. *J Thorac Oncol.* 2007; 2(6):577. <https://doi.org/10.1097/JTO.0b013e318060f16d>. PMID:17545858
5. Huang CY, Ju DT, Chang CF, Reddy PM, Velmurugan BK. A review on the effects of current chemotherapy drugs and natural agents in treating non-small cell lung cancer. *Biomedicine.* 2017; 7(4). <https://doi.org/10.1051/bmdcn/2017070423>. PMID:29130448. PMCID:PMC5682982
6. Jin S, Park HJ, Oh YN, Kwon HJ, Kim JH, Choi YH, *et al.* Anti-cancer activity of *Osmanthus matsumuranus* extract by inducing G2/M arrest and apoptosis in human hepatocellular carcinoma Hep G2 cells. *J Cancer Prev.* 2015; 20(4):241. <https://doi.org/10.15430/JCP.2015.20.4.241>. PMID:26734586. PMCID:PMC4699751
7. Richardson JS, Sethi G, Lee GS, Malek SN. Chalepin: isolated from *Ruta angustifolia* L. Pers induces mitochondrial mediated apoptosis in lung carcinoma cells. *BMC Complement Altern Med.* 2016; 16(1):1-27. <https://doi.org/10.1186/s12906-016-1368-6>. PMID:27729078. PMCID:PMC5059921
8. Mali RG, Dhake AS. Evaluation of effects of *Bauhinia variegata* stem bark extracts against milk-induced eosinophilia in mice. *J. Adv. Pharm. Technol. Res.* 2011; 2(2):132. <https://doi.org/10.4103/2231-4040.82949>. PMID:22171306. PMCID:PMC3217693
9. Katoch D, Sharma JS, Banerjee S, Biswas R, Das B, Goswami D, *et al.* Government policies and initiatives for development of Ayurveda. *J Ethnopharmacol.* 2017; 197:25-31. <https://doi.org/10.1016/j.jep.2016.08.018>. PMID:27543425
10. Aggarwal V, Tuli HS, Varol A, Thakral F, Yerer MB, Sak K, *et al.* Role of reactive oxygen species in cancer progression: Molecular mechanisms and recent advancements. *Biomolecules.* 2019; 9(11):735. <https://doi.org/10.3390/biom9110735>. PMID:31766246. PMCID:PMC6920770

11. Galadari S, Rahman A, Pallichankandy S, Thayyullathil F. Reactive oxygen species and cancer paradox: To promote or to suppress? *Free Radic Biol Med.* 2017; 104:144-64. <https://doi.org/10.1016/j.freeradbiomed.2017.01.004>. PMID:28088622
12. Kirtonia A, Sethi G, Garg M. The multifaceted role of reactive oxygen species in tumorigenesis. *Cell Mol Life Sci.* 2020;1-25.
13. Hensley P, Mishra M, Kyprianou N. Targeting caspases in cancer therapeutics. *Biol. Chem.* 2013; 394(7):831-43. <https://doi.org/10.1515/hsz-2013-0128>. PMID:23509217. PMCid:PMC3721733
14. Jelínek M, Balušíková K, Schmiedlová M, Němcová-Fürstová V, Šrámek J, Stančíková J, et al. The role of individual caspases in cell death induction by taxanes in breast cancer cells. *Cancer Cell Int.* 2015; 15(1):1-6. <https://doi.org/10.1186/s12935-015-0155-7>. PMID:25685064. PMCid:PMC4329194
15. Olsson M, Zhivotovsky B. Caspases and cancer. *Cell Death Differ.* 2011; 18(9):1441-9. <https://doi.org/10.1038/cdd.2011.30>. PMID:21455218. PMCid:PMC3178435
16. Khazaei M, Pazhouhi M. Antiproliferative effect of *Trifolium pratense* L. extract in human breast cancer cells. *Nutr Cancer.* 2019; 71(1):128-40. <https://doi.org/10.1080/01635581.2018.1521443>. PMID:30596276
17. Bhandari J, Muhammad B, Thapa P, Shrestha BG. Study of phytochemical, anti-microbial, anti-oxidant, and anti-cancer properties of *Allium wallichii*. *BMC Complement Altern Med.* 2017; 17(1):1-9. <https://doi.org/10.1186/s12906-017-1622-6>. PMID:28178952. PMCid:PMC5299666
18. Kothari S, Mishra V, Bharat S, Tonpay SD. Antimicrobial activity and phytochemical screening of serial extracts from leaves of *Aegle marmelos* (Linn.). *Acta Pol. Pharm.* 2011; 68(5):687-92.
19. Zhao T, Pan H, Feng Y, Li H, Zhao Y. Petroleum ether extract of *Chenopodium album* L. prevents cell growth and induces apoptosis of human lung cancer cells. *Exp Ther Med.* 2016; 12(5):3301-7. <https://doi.org/10.3892/etm.2016.3765>. PMID:27882153. PMCid:PMC5103781
20. Franken NA, Rodermond HM, Stap J, Haveman J, Van Bree C. Clonogenic assay of cells in vitro. *Nat Protoc.* 2006; 1(5):2315-9. <https://doi.org/10.1038/nprot.2006.339>. PMID:17406473
21. Liang CC, Park AY, Guan JL. In vitro scratch assay: A convenient and inexpensive method for analysis of cell migration in vitro. *Nat Protoc.* 2007; 2(2):329-33. <https://doi.org/10.1038/nprot.2007.30>. PMID:17406593
22. Liu N, Li Y, Su S, Wang N, Wang H, Li J. Inhibition of cell migration by ouabain in the A549 human lung cancer cell line. *Oncol Lett.* 2013; 6(2):475-9. <https://doi.org/10.3892/ol.2013.1406>. PMID:24137350. PMCid:PMC3789103
23. Hsia TC, Yu CC, Hsu SC, Tang NY, Lu HF, Huang YP, et al. Cantharidin induces apoptosis of H460 human lung cancer cells through mitochondria-dependent pathways. *Int J Oncol.* 2014; 45(1):245-54. <https://doi.org/10.3892/ijo.2014.2428>. PMID:24818581
24. Lin W, Ye H. Anticancer activity of ursolic acid on human ovarian cancer cells via ROS and MMP mediated apoptosis, cell cycle arrest and downregulation of PI3K/AKT pathway. *J Buon.* 2020; 25(2):750-56.
25. Alizadeh J, Zeki AA, Mirzaei N, Tewary S, Moghadam AR, et al. Mevalonate cascade inhibition by simvastatin induces the intrinsic apoptosis pathway via depletion of isoprenoids in tumor cells. *Sci Rep.* 2017; 7(1):1-4. <https://doi.org/10.1038/srep44841>. PMID:28344327. PMCid:PMC5366866
26. Bang M, Do Gyeong Kim EL, Kwon KJ, Shin CY. Etoposide induces mitochondrial dysfunction and cellular senescence in primary cultured rat astrocytes. *Biomol Ther.* 2019; 27(6):530. <https://doi.org/10.4062/biomolther.2019.151>. PMID:31646843. PMCid:PMC6824621
27. Elmore S. Apoptosis: A review of programmed cell death. *Toxicol Pathol.* 2007; 35(4):495-516. <https://doi.org/10.1080/01926230701320337>. PMID:17562483. PMCid:PMC2117903
28. Perillo B, Di Donato M, Pezone A, Di Zazzo E, Giovannelli P, Galasso G, et al. ROS in cancer therapy: The bright side of the moon. *Exp Mol Med.* 2020; 52(2):192-203. <https://doi.org/10.1038/s12276-020-0384-2>. PMID:32060354. PMCid:PMC7062874
29. Clark AC, MacKenzie SH. Targeting cell death in tumors by activating caspases. *Curr Cancer Drug Targets.* 2008; 8(2):98-109. <https://doi.org/10.2174/156800908783769391>. PMID:18336192. PMCid:PMC3119715
30. Kumar S. Caspase function in programmed cell death. *Cell Death Differ.* 2007; 14(1):32-43. <https://doi.org/10.1038/sj.cdd.4402060>. PMID:17082813
31. Ji BC, Yu CC, Yang ST, Hsia TC, Yang JS, Lai KC, et al. Induction of DNA damage by deguelin is mediated through reducing DNA repair genes in human non-small cell lung cancer NCI-H460 cells. *Oncol. Rep.* 2012; 27(4):959-64. <https://doi.org/10.3892/or.2012.1622>. PMID:22227970. PMCid:PMC3583480
32. Tiloke C, Phulukdaree A, Chuturgoon AA. The antiproliferative effect of *Moringa oleifera* crude aqueous leaf extract on cancerous human alveolar epithelial cells. *BMC Complement Altern Med.* 2013; 13(1):1-8. <https://doi.org/10.1186/1472-6882-13-226>. PMID:24041017. PMCid:PMC3852616



Research paper

Mononuclear copper(II) and binuclear cobalt(II) complexes with halides and tetradentate nitrogen coordinate ligand: Synthesis, structures and bioactivities



Mehul H. Sadhu^a, Sujit Baran Kumar^{a,*}, Jaswinder Kaur Saini^b, Sejal S. Purani^c, Tanvi R. Khanna^c

^a Department of Chemistry, Faculty of Science, The Maharaja Sayajirao University of Baroda, Vadodara 390002, India

^b Department of Microbiology and Biotechnology Centre, Faculty of Science, The Maharaja Sayajirao University of Baroda, Vadodara 390002, India

^c Department of Biochemistry, Faculty of Science, The Maharaja Sayajirao University of Baroda, Vadodara 390002, India

ARTICLE INFO

Article history:

Received 17 March 2017
Received in revised form 13 May 2017
Accepted 2 June 2017
Available online 3 June 2017

Keywords:

Tripodal ligand
Copper(II) and cobalt(II) complexes
Spectra
Structure
Bioactivities

ABSTRACT

In this work, we present the synthesis of four mononuclear copper(II) complexes [Cu(bdpab)X]Y and two binuclear cobalt(II) complexes [Co(bdpab)Cl]₂Y₂ (X = Cl⁻, Br⁻; Y = PF₆⁻, BF₄⁻) with tripodal N₄-coordinate N-benzyl-N',N'-bis(3,5-dimethyl-1H-pyrazol-1-yl)-2-methyl-1,2-ethylenediamine (bdpab) and the complexes were characterized by elemental analyses, IR spectral data, molar conductivity measurement, EPR and crystal structure determination. Single crystal X-ray diffraction studies indicate that the copper centers in the complexes [Cu(bdpab)Cl]PF₆ and [Cu(bdpab)Br]PF₆ have distorted square pyramidal geometry and complex [Co(bdpab)Cl]₂(PF₆)₂ has octahedral geometry and two [Co(bdpab)Cl]⁺ units are linked by two (μ-Cl) bridges. Copper(II) complexes form 1D supramolecular chain along c-axis through C-H-π interaction whereas cobalt(II) complex form 1D supramolecular chain along a-axis through π-π interaction. The antimicrobial activity of complexes [Cu(bdpab)Cl]PF₆, [Cu(bdpab)Br]PF₆ and [Co(bdpab)Cl]₂(PF₆)₂ were investigated against gram positive (*Bacillus subtilis*, *Streptococcus aureus*) and gram negative (*Escherichia coli*, *Pseudomonas aeruginosa*) bacterial strains by agar well dilution method and have demonstrated significant antimicrobial activity of the compounds. [Co(bdpab)Cl]₂(PF₆)₂ exhibited the best antibacterial activity among all the synthesized complexes. The studies on the interaction of complexes and DNA by agarose gel electrophoresis method revealed that the complexes can effectively cleave the circular plasmid DNA at very low concentrations. The cytotoxic activity of the complexes against A549 lung cancer cells showed that the complexes have better cytotoxic activity than corresponding metal salts and [Cu(bdpab)Br]PF₆ complex has best cytotoxic activity among the synthesized complexes.

© 2017 Elsevier B.V. All rights reserved.

1. Introduction

Since the discovery of cis-platin as an anti-cancer agent, design and synthesis of new transition metal compounds and their interaction with DNA have been an important area of research in bioinorganic chemistry for the development of new material as the therapeutic agent [1–4]. It is well known that gene has important role in the biological process and the study of the interaction of DNA with transition metal complexes is important for the development of less toxic, target specific and less side effect of the transition metal containing metallodrug [5–7]. Transition metal complexes are used as bioactive complex because they have different binding ability, coordination numbers and oxidation states etc.

Among the transition metal complexes investigated as therapeutic agent, majority are from copper as it is an essential element for the biological system and has low toxicity [8–16]. Since cobalt is also important elements in the bio system, the interaction of cobalt with DNA has been attracted recently [17,18]. Since the DNA and transition metal interaction depends on the donor atom of the ligand, nitrogen coordinating ligands such as poly-pyridine are used mostly for the synthesis of bioactive transition metal complexes [19,20]. Many copper(II) and cobalt(II) complexes with tripodal ligands have been investigated for their anticancer properties [21–23]. There are few reports on the bioactivities on the model complexes of bleomycin with imidazole, pyrimidinyl amino and amino donor groups of ligands [24–26]. Since there are some similarities between the metal binding of model complexes and metal complexes with tripodal pyrazole-based N₄-tetradentate ligands, we are interested to study the bioactivities of the copper(II) and cobalt(II) complexes with this pyrazolyl containing ligand.

* Corresponding author.

E-mail address: sujit_baran@yahoo.com (S.B. Kumar).

In this paper we report on the synthesis, characterization, structures and bioactivities of mononuclear copper(II) complexes $[\text{Cu}(\text{bdpad})\text{X}]\text{Y}$ and binuclear cobalt(II) complexes $[\text{Co}(\text{bdpab})\text{Cl}]_2(\text{Y})_2$ ($\text{X} = \text{Cl}$ or Br and $\text{Y} = \text{BF}_4$ or PF_6). Crystal structures of three complexes $[\text{Cu}(\text{bdpab})\text{Cl}]\text{PF}_6$, $[\text{Cu}(\text{bdpab})\text{Br}]\text{PF}_6$ and $[\text{Co}(\text{bdpab})\text{Cl}]_2(\text{PF}_6)_2$ have been solved by single crystal X-ray diffraction method. Antimicrobial activity, cytotoxicity and DNA cleavage study of the complexes have been investigated in detail.

2. Experimental

2.1. Materials

All chemicals and solvents were analytical grade reagents and purchased from commercial sources. Acetylacetone, paraformaldehyde, hydrazine hydrate, $\text{CuCl}_2 \cdot 2\text{H}_2\text{O}$, $\text{CuBr}_2 \cdot 4\text{H}_2\text{O}$ (Loba, India), $\text{CoCl}_2 \cdot 6\text{H}_2\text{O}$ (Siscochem, India), NH_4BF_4 and NH_4PF_6 (Aldrich) were reagent grade and used as received. *N*-(3,5-dimethyl-1H-pyrazol-1-yl)methanol [27] *N*-benzyl-*N'*-bis(3, 5-dimethyl-1H-pyrazol-1-yl)-2-methyl-1,2-ethylenediamine (bdpab) were synthesized as per the published procedures [28].

2.2. Cell line and culture

Human lung carcinoma (A549) cells were procured from National Centre for Cell Science, Pune, India. The cell cultures were grown in Dulbecco's modified Eagle's medium (DMEM, Himedia) supplemented with 10% fetal bovine serum (Gibco-Invitrogen) and 1% antibiotic (Gibco-Invitrogen). Cell lines were maintained at 37 °C in a 5% (v/v) CO_2 atmosphere with 95% (v/v) humidity in a humidified incubator (Thermo Scientific). Cultures were passaged weekly using trypsin-EDTA (Himedia) to detach the cells from their culture flasks. The copper(II) and cobalt(II) salts and their complexes were dissolved in DMSO and diluted to the required concentration with culture medium. The DMSO content in the final concentrations did not exceed 0.1%.

2.3. Antimicrobial activity assay

The antimicrobial activity of the complexes were determine using various concentrations of Cu(II) and the complexes were prepared in distilled water with not more than 0.1% DMSO to assist dissolution. The screening was carried out using Gram positive (*Bacillus subtilis*, *Streptococcus aureus*) and Gram negative (*Escherichia Coli*, *Pseudomonas aeruginosa*) bacterial strains by agar well diffusion method. All the compounds were tested in duplicates. The Luria Bertani (LB) agar plates with 4 mm thickness were spread with 100 μl of overnight cultures. The test compounds at different concentrations were added to the wells (5 mm diameter) made in the agar plates. DMSO at the concentration of 0.1% was used as a negative control and 1 mg/mL of chloramphenicol was used as a positive control for the assay. The plates were incubated at 37 °C for 24 h. The plates were checked for zones of inhibition after incubation.

2.4. Cell proliferation assay (MTT)

Cell proliferation assay was performed [29] to check the in vitro anticancer activities of the two copper(II) and cobalt(II) salts and their complexes against A549 lung cancer cell line. The cells were seeded in 96-well microplates at a concentration of 5×10^4 cells/well. In the 24th hour, the fresh media modified with different concentrations of the test compounds was added. Each concentration was applied in triplicates. Untreated A549 cells grown in non-modified medium served as control. After 24 h incubation, the solutions

were removed from the plates and (3-(4,5-dimethylthiazol-2-yl)-2,5-diphenyltetrazolium bromide) (MTT) (5 mg/mL DMEM) solution was added followed by 3 h incubation. Medium with MTT was flicked off and the formazan crystals were solubilized in 100 μl DMSO. The absorbance of each well was measured at 540/620 nm by ELISA microplate reader (Thermo Scientific). Relative cell viability, expressed as a percentage of the untreated control (100% viability), was calculated for each concentration. Concentration-response curves were constructed for each experiment. The data are presented as means \pm standard error of the mean. The IC_{50} values were calculated from the curves constructed by plotting cell survival (%) vs the complexes concentration ($\mu\text{g/mL}$). Statistical differences between control and treated cells at different concentrations were assessed by 2-way anova test in Graph-Pad Prism 5.0 software package.

2.5. Cleavage experiment

The bacterial plasmid pBS KS (+) was isolated from *Escherichia coli* strain by alkaline lysis method [30]. The ratio 260 to 280 nm (A_{260}/A_{280}) absorbance was checked to be ~ 1.86 , which indicated that the DNA is sufficiently free from protein [31]. The concentration of DNA was determined spectrophotometrically (UV 1601 UV-Visible spectrophotometer, SHIMADZU) at 260 nm using the known molar extinction coefficient value of $6700 \text{ M}^{-1} \text{ cm}^{-1}$ [32]. The DNA was stored at -20°C until used. Visualization of DNA under UV was done using Alpha imager HP System, Alpha innotech.

The Cu(II) complexes **1**, **3** and **5** were examined for their ability to cleave DNA. For this 3 μM pBS KS(+) plasmid DNA was treated with Cu(II) complexes at various concentration ranging from 10 μM –50 μM along with the addition of 5 μM hydrogen peroxide. A plasmid with volume made up with sterile distilled water was kept as an untreated control. A reaction with 5 μM H_2O_2 alone and with 50 μM of the complexes alone were also kept to check their individual effect on the plasmid. After overnight incubation at 37 °C, 5 μl from each reaction was loaded using bromophenol blue (0.25%) and glycerol (30%) loading dye onto 0.8% agarose gel containing ethidium bromide (final 0.5 $\mu\text{g/ml}$). The gel was observed under UV trans illuminator at 360 nm.

2.6. Syntheses

2.6.1. Synthesis of complex $[\text{Cu}(\text{bdpab})\text{Cl}]\text{PF}_6$ (**1**)

A solution of ligand bdpab (0.176 g, 0.5 mmol) in methanol (10 ml) was added drop by drop to a stirred light green solution of $\text{CuCl}_2 \cdot 2\text{H}_2\text{O}$ (0.085 g, 0.5 mmol) in the same solvent (10 ml) and the colour changed to dark green immediately. After 10 min, NH_4PF_6 (0.082 g, 0.5 mmol) in methanol (10 ml) was added drop by drop and resulting green color solution was stirred for another 3 h at room temperature, filtered it and kept the filtrate for slow evaporation at room temperature. Light green color single crystals were obtained after 5 days.

Yield. 0.110 g (74%). Found C = 40.78, H = 4.88, N = 14.21%. Anal calc for $\text{C}_{20}\text{H}_{28}\text{ClCuF}_6\text{N}_6\text{P}$: C = 40.27, H = 4.73, N = 14.09%. IR (KBr pellet) cm^{-1} : $\nu(-\text{NH})$, 3329 vs; $\nu(\text{C}=\text{C})/\text{ph}$ ring, 1600 s; $\nu(\text{C}=\text{C}) + \nu(\text{C}=\text{N})/\text{pz}$ ring 1551 s, 1474 s; $\nu(\text{PF}_6^-)$, 848 s. UV-Vis spectra: $\lambda_{\text{max}}/\text{nm}$ ($\epsilon_{\text{max}}/\text{mol}^{-1}\text{cm}^{-1}$). 682(171), 279(4568), 226(18067). Λ_{M} ($\Omega^{-1}\text{cm}^2 \text{ mol}^{-1}$) = 120. μ_{eff} = 1.76 BM.

2.6.2. Synthesis of complex $[\text{Cu}(\text{bdpab})\text{Cl}]\text{BF}_4$ (**2**)

This complex was prepared by following the same procedure as that of complex **1** except NH_4BF_4 was used in place of NH_4PF_6 .

Yield. 0.105 g (77%). Found C = 44.77, H = 5.32, N = 15.78%. Anal calc for $\text{C}_{20}\text{H}_{28}\text{ClCuF}_4\text{N}_6\text{B}$: C = 44.63, H = 5.24, N = 15.61%. IR (KBr pellet) cm^{-1} : $\nu(-\text{NH})$, 3132 vs; $\nu(\text{C}=\text{C})/\text{ph}$ ring, 1600 s; $\nu(\text{C}=\text{C}) +$

$\nu(\text{C}=\text{N})/\text{pz}$ ring, 1555 s, 1476 s; $\nu(\text{BF}_4^-)$, 1055 br. UV–Vis spectra: $\lambda_{\text{max}}/\text{nm}$ ($\epsilon_{\text{max}}/\text{mol}^{-1}\text{cm}^{-1}$). 672(302), 274(4695), 220(15550). Λ_{M} ($\Omega^{-1}\text{cm}^2\text{mol}^{-1}$) = 120. μ_{eff} = 1.78 BM.

2.6.3. Synthesis of complex [Cu(bdpab)Br]PF₆ (3)

This complex was prepared by following the same procedure as that of complex **1** except CuBr₂·4H₂O was used in place of CuCl₂·2H₂O.

Yield. 0.136 g (85%). Found C = 37.20, H = 4.28, N = 13.03%. Anal calc for C₂₀H₂₈BrCuF₆N₆P: C = 37.48, H = 4.40, N = 13.11%. IR (KBr pellet) cm⁻¹; $\nu(-\text{NH})$, 3242 vs; $\nu(\text{C}=\text{C})/\text{ph}$ ring, 1603 s; $\nu(\text{C}=\text{C}) + \nu(\text{C}=\text{N})/\text{pz}$ ring 1558 s, 1476 s; $\nu(\text{PF}_6^-)$, 839 s. UV–Vis spectra: $\lambda_{\text{max}}/\text{nm}$ ($\epsilon_{\text{max}}/\text{mol}^{-1}\text{cm}^{-1}$). 703(202), 303(4241), 225(19673). Λ_{M} ($\Omega^{-1}\text{cm}^2\text{mol}^{-1}$) = 120. μ_{eff} = 1.71 BM.

2.6.4. Synthesis of complex [Cu(bdpab)Br]BF₄ (4)

This complex was prepared by following the same procedure as that of complex **1** except CuBr₂·4H₂O and NH₄BF₄ was used in place of CuCl₂·2H₂O and NH₄PF₆.

Yield. 0.117 g (80%). Found C = 41.58, H = 4.72, N = 14.35%. Anal calc for C₂₀H₂₈BrCuF₄N₆B: C = 41.22, H = 4.84, N = 14.42%. IR (KBr pellet) cm⁻¹; $\nu(-\text{NH})$, 3326 vs; $\nu(\text{C}=\text{C})/\text{ph}$ ring, 1633 s; $\nu(\text{C}=\text{C}) + \nu(\text{C}=\text{N})/\text{pz}$ ring 1553 s, 1470 s; $\nu(\text{BF}_4^-)$, 1042 br. UV–Vis spectra: $\lambda_{\text{max}}/\text{nm}$ ($\epsilon_{\text{max}}/\text{mol}^{-1}\text{cm}^{-1}$). 709(237), 301(3724), 221(20200). Λ_{M} ($\Omega^{-1}\text{cm}^2\text{mol}^{-1}$) = 120. μ_{eff} = 1.73 BM.

2.6.5. Synthesis of complex [Co(bdpab)Cl]₂(PF₆)₂ (5)

Ligand bdpab(0.176 g, 0.5 mmol) in methanol (10 ml) was drop by drop added to a stirring solution of CoCl₂·6H₂O (0.120 g, 0.5 mmol) in the same solvent (10 ml) and the colour changed from light pink to light blue. After 10 min, NH₄PF₆ (0.082 g, 0.5 mmol) in methanol (10 ml) was added drop by drop in the solution. The resulting light blue color solution was stirred for further 3 h at room temperature, filtered and the filtrate was kept for slow evaporation. Light pink color single crystals were obtained after one week.

Yield. 0.077 g (52%). Found C = 40.72, H = 4.86, N = 14.18%. Anal calc for C₄₀H₅₆Cl₂Co₂F₁₂N₁₂P₂: C = 40.59, H = 4.77, N = 14.20%. IR (KBr Pellet) cm⁻¹; $\nu(-\text{NH})$, 3197 vs; $\nu(\text{C}=\text{C})/\text{ph}$ ring, 1603 s; $\nu(\text{C}=\text{C}) + \nu(\text{C}=\text{N})/\text{pz}$ ring 1556 s, 1476 s; $\nu(\text{PF}_6^-)$, 840 s. UV–Vis spectra: $\lambda_{\text{max}}/\text{nm}$ ($\epsilon_{\text{max}}/\text{mol}^{-1}\text{cm}^{-1}$). 830(54), 628(207), 607(349), 531(234), 501(271), 245(17259). Λ_{M} ($\Omega^{-1}\text{cm}^2\text{mol}^{-1}$) = 120. μ_{eff} = 4.37 BM.

2.6.6. Synthesis of complex [Co(bdpab)Cl]₂(BF₄)₂ (6)

This complex was prepared by following the same procedure as that of complex **5** except NH₄BF₆ was used in place of NH₄PF₆.

Yield. 0.081 g (60%). Found C = 45.35, H = 5.37, N = 15.64%. Anal calc for C₄₀H₅₆Cl₂Co₂F₈N₁₂B₂: C = 45.01, H = 5.29, N = 15.75%. IR (KBr pellet) cm⁻¹; $\nu(-\text{NH})$, 3197 vs; $\nu(\text{C}=\text{C})/\text{ph}$ ring, 1603 s; $\nu(\text{C}=\text{C}) + \nu(\text{C}=\text{N})/\text{pz}$ ring 1556 s, 1476 s; $\nu(\text{PF}_6^-)$, 840 s. UV–Vis spectra: $\lambda_{\text{max}}/\text{nm}$ ($\epsilon_{\text{max}}/\text{mol}^{-1}\text{cm}^{-1}$). 829(33), 632(109), 605(274), 530(182), 501(201), 246(26217). Λ_{M} ($\Omega^{-1}\text{cm}^2\text{mol}^{-1}$) = 122. μ_{eff} = 4.36 BM

2.7. Physical measurements

The IR spectra were recorded on a PerkinElmer FT-IR spectrometer RX1 spectrum using KBr pellets. The micro analyses (C, H and N) were carried out using a Perkin Elmer IA 2400 series elemental analyzer. UV–Vis spectra (1100–190 nm) of all complexes were recorded on a JASCO V630 (Spectrophotometer) in CH₃CN solution (~10⁻³ M). Solution conductivity were measured in CH₃CN solution (~10⁻³ M) using Equip-Tronics conductivity meter (model No. EQ-660A). Room temperature magnetic susceptibilities of powder samples were measured using a Faraday magnetic balance

equipped with a Metler UMX 5 balance, OMEGA temperature controller with a field strength of 0.8 T using Hg [Co(SCN)₄] as the reference. X-band EPR measurements were measured on a Bruker EMX EPR spectrometer at liquid nitrogen temperature (77 K).

2.8. Crystal structure determination

The details of crystal structure determination, data collection, crystal data and some important features of the refinements parameters for complex **1**, **3** and **5** are listed in Table 1 and selected bond lengths and angles are given in Table 2. Crystals of suitable size were obtained by slow evaporation of methanol solution of the compounds. Data were collected with Mo-K_α radiation ($\lambda = 0.71073 \text{ \AA}$) (graphite monochromator) for all complexes at 110 K on an Oxford X-CALIBUR-S diffractometer equipped with a CCD area detector. The intensity data were collected using ω and ϕ scans with frame width of 0.5°. The data interpretations were processed with CrysAlisPro, Agilent Technologies, Version 1.171.35.19 [33] and an absorption correction based on the multi-scan method was applied [34]. The reported structures were solved by direct methods and refined by full-matrix least-squares based on F^2 technique using the SHELXL-97 program package [35]. All calculations were carried out using WinGX system Ver-1.64 [36]. All non-hydrogen atoms were refined anisotropically. The positions of the hydrogen atoms were calculated from the difference Fourier map, placed in the calculated positions and constrained to ride on their parent atoms. ORTEP3 for Windows program were used for generating the structures [37].

3. Results and discussion

Four mononuclear five coordinated copper(II) complexes [Cu(bdpab)X]Y and two binuclear six coordinate Co(II) complexes [Co₂(bdpab)₂(μ-Cl)₂]Y₂ (where X = Cl⁻, Br⁻ and Y = PF₆⁻, BF₄⁻) were synthesized through the one-pot reaction of metal halides, ligand bdpab and NH₄PF₆/NH₄BF₄ in the 1:1:1 mol ratio respectively, in methanol at room temperature [scheme 1]. All the complexes were obtained in good yield and characterized by elemental analysis, UV–Vis, IR, EPR and single crystal X-ray diffraction studies. The ligand bdpab is tetradentate and has utilized its all four nitrogen donor atoms for coordination with metal ions. The coordination of ligand bdpab was confirmed by IR and single crystal X-ray diffraction studies (Figs. 1(a), 2(a) and 3(a)). Suitable crystal of complexes **1**, **3** and **5** were obtained by slow evaporation of solvent at room temperature. Single crystal X-ray data revealed that all copper(II) complexes are mononuclear five coordinated with distorted square pyramidal geometry whereas cobalt(II) complexes are binuclear with distorted octahedral geometry. Molar conductivity data in CH₃CN solution show all the complexes have 1:1 electrolyte ($\Lambda_{\text{M}} = 120 \Omega^{-1}\text{cm}^2\text{mol}^{-1}$) which support the presence of counter anion outside the coordination sphere [38]. All complexes are air stable and soluble in organic solvent like methanol, ethanol, acetonitrile etc.

3.1. IR spectral data

The preliminary analysis of all complexes were characterized from their IR spectra. One medium intensity band was observed at ~3200 cm⁻¹ due to secondary amine(-NH) group and two medium intensity bands at ~1553 and ~1464 cm⁻¹ were due to pyrazolyl $\nu(\text{C}=\text{C}) + \nu(\text{C}=\text{N})$ group of the ligand (bdpab) and these bands are also present in the IR spectra of ligand with the little difference in frequency indicating the coordination of the ligand to the metal centers. IR spectra of the complexes **1**, **3** and **5** show an intense band at ~845 cm⁻¹ confirming the presence of $\nu(\text{PF}_6^-)$

Table 1
Crystallographic parameters of the complexes **1**, **3** and **5**.

	[Cu(bdpab)Cl]PF ₆ (1)	[Cu(bdpab)Br]PF ₆ (3)	[Co(bdpab)Cl] ₂ (PF ₆) ₂ (5)
Empirical formula	C ₂₀ H ₂₈ ClCuF ₆ N ₆ P	C ₂₀ H ₂₈ BrCuF ₆ N ₆ P	C ₄₀ H ₅₆ Cl ₂ Co ₂ F ₁₂ N ₁₂ P ₂
Formula weight	596.44	640.90	1183.67
Temperature (K)	110(10)	110(2)	110(15)
Wavelength (Å)	0.71073	0.71073	0.71073
Crystal system	triclinic	triclinic	triclinic
Space group	<i>P</i> -1	<i>P</i> -1	<i>P</i> -1
<i>a</i> (Å)	9.9493(7)	10.1081(3)	9.6899(3)
<i>b</i> (Å)	10.2231(6)	10.1360(3)	10.8074(5)
<i>c</i> (Å)	13.0782(7)	13.1339(3)	13.1823(5)
α (°)	103.917(5)	106.148(2)	103.944(3)
β (°)	106.243(5)	103.355(2)	102.545(3)
γ (°)	101.402(5)	101.043(2)	105.951(3)
Volume (Å ³)	1188.47(13)	1209.58(6)	1227.36(9)
<i>Z</i>	2	2	1
Density (Mg/m ³)	1.667	1.760	1.6013
Absorption coefficient (μ) (mm ⁻¹)	1.168	2.689	0.941
F(000)	610.0	646.0	606.0
Crystal size (mm)	0.25 × 0.17 × 0.12	0.25 × 0.17 × 0.12	0.28 × 0.18 × 0.14
Theta range for data collection (°)	6.14 to 57.9	6.24 to 58.16	6.44 to 58.02
Index ranges	-13 ≤ <i>h</i> ≤ 12, -13 ≤ <i>k</i> ≤ 12, -16 ≤ <i>l</i> ≤ 17	-13 ≤ <i>h</i> ≤ 13, -12 ≤ <i>k</i> ≤ 13, -17 ≤ <i>l</i> ≤ 17	-13 ≤ <i>h</i> ≤ 13, -14 ≤ <i>k</i> ≤ 14, -17 ≤ <i>l</i> ≤ 17
Reflections collected	10336	26896	26806
Independent reflections	6298	6482	6527
Data/restraints/parameters	6298/0/320	6482/0/320	6527/0/323
Goodness-of-fit on <i>F</i> ²	1.050	1.051	0.906
Final R indices [<i>I</i> > 2σ(<i>I</i>)]	R1 = 0.0447, wR2 = 0.1094	R1 = 0.0352, wR2 = 0.0857	R1 = 0.0387, wR2 = 0.1164
R indices (all data)	R1 = 0.0553, wR2 = 0.1151	R1 = 0.0419, wR2 = 0.0891	R1 = 0.0495, wR2 = 0.1244
Largest diff. peak and hole (eÅ ⁻³)	0.80 and -0.66	0.73 and -0.69	0.74 and -0.87

counter anion and complexes **2,4** and **6** exhibited a broad band at ~1065 cm⁻¹ indicating the presence of ν(BF₄⁻) counter anion [39].

3.2. Electronic Spectra, EPR and magnetic data

The UV–Visible spectra of all the complexes **1–6** were recorded in CH₃CN (10⁻³ M) in the range of 200–1100 nm. The high intensity bands appeared at <400 nm are due to intra ligand n-π* and π-π* charge transfer transition. In the visible region, a broad absorption band was observed at λ > 670 nm due to d_{xy}, d_{yz} → d_{xy}² for all copper (II) complexes. This type of spectral feature is typical for Cu(II) complexes with square pyramidal geometry. Generally, trigonal bipyramidal Cu(II) complexes show two spectral bands in the region of 700–750 nm (due to d_{xy}, d_{yz} → d_{xy}²) and at 800–870 nm (due to d_{xy}, d_{xy}² → d_{xy}²) transition. Absence of spectral band in the two regions in the compounds also support the geometry around copper(II) center is distorted square pyramidal [40,41]. For cobalt(II) complexes, the three absorption bands appeared at 830, ~630, ~530 nm for complexes **5** and **6** and these are due to d-d transition or ligand field transitions. This type of transitions are generally observed for high spin cobalt(II) complexes.

The X-band EPR spectra of the complexes **1** and **3** in acetonitrile solution (78 K) show four-line splitting pattern with g_{||} = 2.244 and g_⊥ = 2.042 for complex **1** and with g_{||} = 2.252 and g_⊥ = 2.051 for complex **2**, indicating the interaction of the unpaired electron with nuclear spin of the copper(II) nucleus (^{63,65}Cu; I = 3/2). The g_{||} value is greater than g_⊥, indicating a pseudotetragonal site symmetry of the copper(II) in the complexes.

Room temperature magnetic susceptibility measurements of powder sample of the complexes show that the complexes have magnetic moments close to their spin only value for Cu(II) complexes (S = 1/2) with μ_{eff} ~ 1.75 BM indicating one electron paramagnetism, for Co(II) complexes (S = 3/2) with μ_{eff} ~ 4.37 BM indicating three electron paramagnetism, respectively. In general,

magnetic moment of cobalt(II) complex with tetradentate N₄-coordinate ligand fall in this region [42,43].

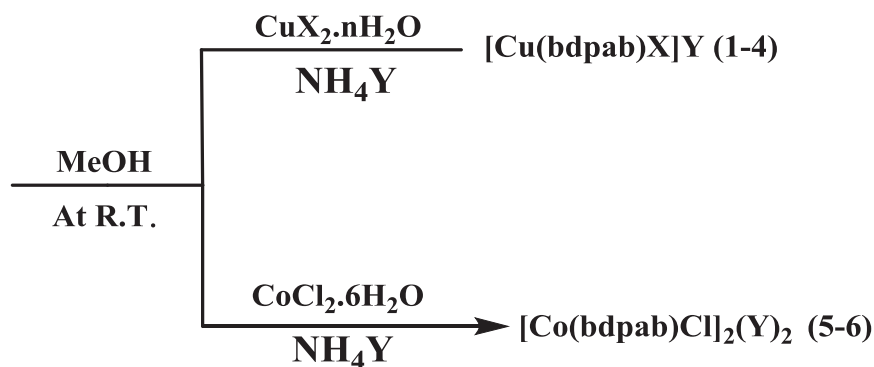
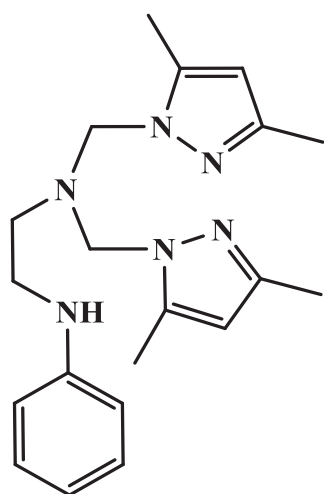
3.3. Crystal structures

3.3.1. Crystal structures of [Cu(bdpab)X]PF₆ [X = Cl(**1**), Br(**3**)]

The structural analyses show that both complexes **1** and **3** crystallize in the triclinic crystal system with the *P*-1 space group and consist of two mononuclear motifs in packing which are further engaged with CH-π and π-π interaction among themselves to give supramolecular 1D structures. An ORTEP diagrams with the atom labelling scheme of the monomeric cations [Cu(bdpab)Cl]⁺ of (**1**) and [Cu(bdpab)Br]⁺ of (**3**) are shown in Figs. 1(a) and 2(a). A summary of the X-ray crystallographic data and selected bond distance and angles are given in Table. 2. In both complexes, the copper(II) center has five coordination- four coordination from nitrogen atoms [N(1), N(2), N(3), N(6)] of ligand bdpab and the remaining position occupied by respective halides [Cl(1) or Br(1)]. So the environment around five coordinated copper(II) center can be described as a structure between square-pyramidal (SP) and trigonal-bipyramidal (TBP). Addison et al. defined the angular structural index geometric parameter [τ = (β - α)/60] (where β and α are the two largest angles of the metal coordination sphere) which is applicable to five co-ordinate structures as an index of the degree of trigonality. The parameter has been used to describe the degree of structural distortion from the SP geometry (τ = 0) to the TBP geometry (τ = 1) [44]. The value of Addison parameter τ are 0.17 and 0.16 for complexes **1** and **3**, respectively, indicating that copper(II) center in both complexes were adopted slightly distorted square pyramidal geometry. In square pyramidal (4+1) geometry, the basal plane formed by two pyrazole nitrogen N(3) and N(6), one tertiary nitrogen N(2) from ligand bdpab and one halide X(1) [X = Cl(1) or Br(1)] and secondary nitrogen atom N(1) from ligand bdpab coordinates axially at a long distance to copper(II) center in the complexes. For both complexes, the chelate

Table 2
Important bond lengths (Å) and bond angles (°) of complexes **1**, **3** and **5**.

Bond lengths (Å)					
[Cu(bdpab)Cl]PF₆ (1)		[Cu(bdpab)Br]PF₆ (3)		[Co(bdpab)Cl]₂(PF₆)₂ (5)	
Cu(1)-N(3)	1.977(3)	Cu(1)-N(6)	1.983(2)	Co(1)-N(2)	2.2324(17)
Cu(1)-N(6)	1.982(3)	Cu(1)-N(3)	1.988(2)	Co(1)-N(3)	2.1233(17)
Cu(1)-N(2)	2.114(2)	Cu(1)-N(2)	2.123(2)	Co(1)-N(5)	2.1303(17)
Cu(1)-N(1)	2.410(3)	Cu(1)-N(1)	2.391(2)	Co(1)-N(1)	2.2245(18)
Cu(1)-Cl(1)	2.2404(8)	Cu(1)-Br(1)	2.3783(4)	Co(1)-Cl(1)	2.4786(5)
				Co(1)-Cl(1i)	2.4259(5)
				Co(1)-Co(1i)	3.607
Bond angles (°)					
[Cu(bdpab)Cl]PF₆ (1)		[Cu(bdpab)Br]PF₆ (3)			
N(3)-Cu(1)-N(6)	161.24(10)	N(6)-Cu(1)-N(3)	160.82(9)		
N(3)-Cu(1)-N(2)	79.85(10)	N(6)-Cu(1)-N(2)	79.54(8)		
N(6)-Cu(1)-N(2)	82.26(10)	N(3)-Cu(1)-N(2)	82.27(8)		
N(3)-Cu(1)-Cl(1)	97.40(8)	N(6)-Cu(1)-Br(1)	96.98(6)		
N(6)-Cu(1)-Cl(1)	99.46(8)	N(3)-Cu(1)-Br(1)	100.04(6)		
N(2)-Cu(1)-Cl(1)	171.25(7)	N(2)-Cu(1)-Br(1)	170.59(6)		
N(3)-Cu(1)-N(1)	92.27(10)	N(6)-Cu(1)-N(1)	92.09(9)		
N(6)-Cu(1)-N(1)	90.54(10)	N(3)-Cu(1)-N(1)	91.21(8)		
N(2)-Cu(1)-N(1)	81.22(9)	N(2)-Cu(1)-N(1)	81.56(8)		
Cl(1)-Cu(1)-N(1)	107.27(7)	Br(1)-Cu(1)-N(1)	107.41(5)		
[Co(bdpab)Cl]₂(PF₆)₂ (5)					
N(3)-Co(1)-N(2)		77.40(6)			
N(5)-Co(1)-N(2)		76.35(6)			
N(5)-Co(1)-N(3)		153.71(7)			
N(1)-Co(1)-N(2)		80.10(6)			
N(1)-Co(1)-N(3)		89.35(7)			
N(1)-Co(1)-N(5)		87.56(7)			
Cl(1i)-Co(1)-N(2)		178.03(4)			
Cl(1)-Co(1)-N(2)		95.77(4)			
Cl(1i)-Co(1)-N(3)		104.24(5)			
Cl(1)-Co(1)-N(3)		91.34(5)			
Cl(1)-Co(1)-N(5)		89.89(5)			
Cl(1i)-Co(1)-N(5)		102.04(5)			
Cl(1)-Co(1)-N(1)		175.56(5)			
Cl(1i)-Co(1)-N(1)		98.76(5)			
Co(1)-Cl(1)-Co(1i)		94.67			



Where, $n = 2$ (For $\text{X} = \text{Cl}^-$), 4 (For $\text{X} = \text{Br}^-$)

$\text{Y} = \text{PF}_6^-, \text{BF}_4^-$.

Scheme 1. Synthesis of complexes.

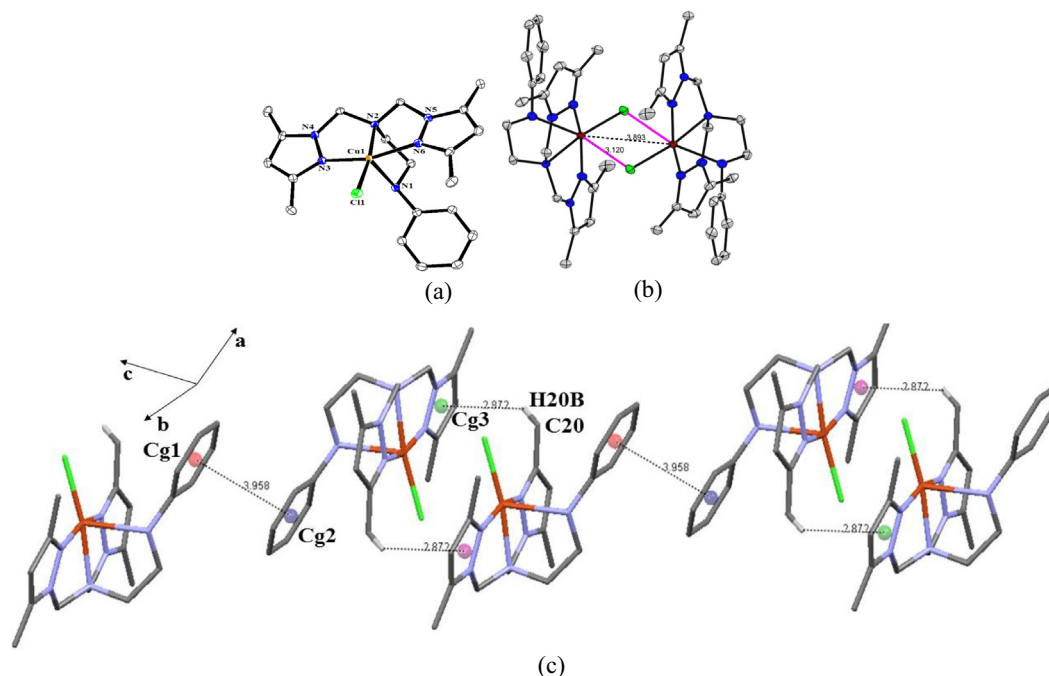


Fig. 1. (a) ORTEP diagram depicting the cationic part of the complex **1** with atom numbering scheme (40% probability factor for the thermal ellipsoids). (b). Perspective view of the supramolecular dimer $[\{Cu(bdpab)Cl\}]^{2+}$ of **1**. (c). Intermolecular interaction of complex **1**.

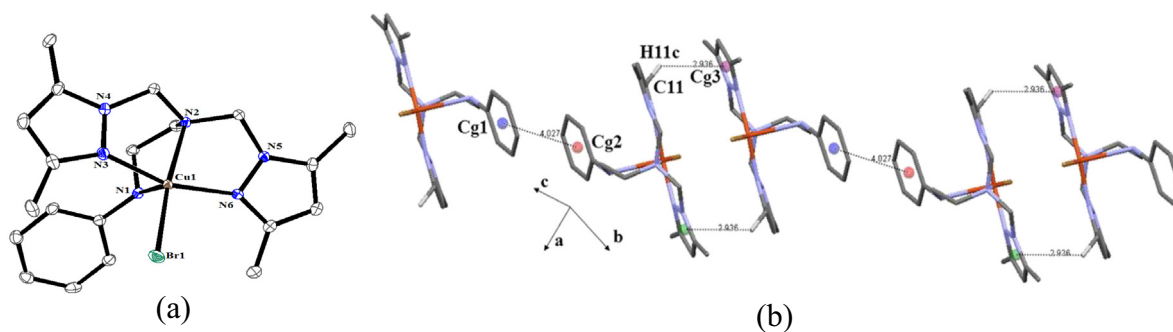


Fig. 2. (a) ORTEP diagram depicting the cationic part of the complex **3** with atom numbering scheme (40% probability factor for the thermal ellipsoids). (b). Intermolecular interaction of complex **3**.

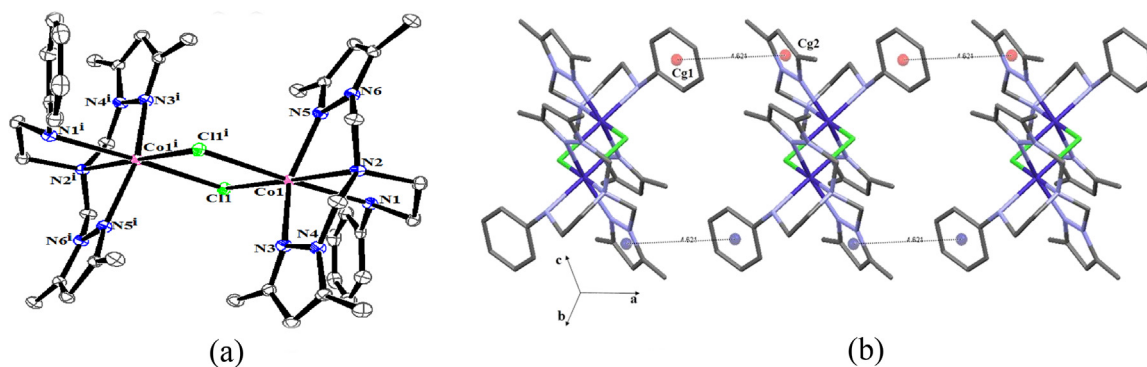


Fig. 3. (a) ORTEP diagram depicting the cationic part of the complex **5** with atom numbering scheme (40% probability factor for the thermal ellipsoids). (b). Intermolecular interaction of complex **5**.

ligand is coordinated in a neutral form in a tetradentate N_4 manner, via two pyrazole nitrogen atoms N(3) and N(6), one tertiary nitrogen atom N(2) and one secondary aniline nitrogen atom N(1) forming three fused five-membered chelate rings.

For complex **1**, equatorial bond distances of Cu–N(2) [2.114(2) Å], Cu(1)–N(3) [1.977(3) Å], Cu(1)–N(6) [1.982(3) Å] and Cu(1)–Cl(1) [2.2404(8) Å] are not same and axial position is occupied by secondary nitrogen N(1) with long Cu–N(1) [2.410(3) Å]

distance. Deviations of coordinating atoms N(2), N(3), N(6) and Cl(1) from the mean plane are 0.049, 0.0076, 0.009 and 0.048 Å, respectively. In this square pyramidal structure, the copper(II) is slightly displaced 0.112 Å out of this mean square plane towards the secondary amine nitrogen of ligand bdpab. The chelate bite angles for three five membered chelate rings, N(1)–Cu(1)–N(2), N(2)–Cu(1)–N(3) and N(2)–Cu(1)–N(6) are 171.25(7), 79.85(10) and 82.26(10), respectively. These bond angles and distances are comparable to previously reported chloride and N_4 -coordinated tripodal ligand containing copper(II) complex [45,46].

The shortest Cu—Cu separation is 3.893 Å and the Cu(1)—Cl(1)[2-x, 1-y, 2-z] separation is 3.120 Å, thus formation of supramolecular dimer is observed [Fig. 1(b)]. Two molecules in a unit cell are attached together through $\pi \dots \pi$ stacking between the two phenyl rings of two nearest ligand bdpab with distance between the two centroids Cg(1)–Cg(2) is 3.958 Å and C–H... π interactions between one hydrogen atom of –CH₃ group attached with pyrazole ring of one ligand and nearest pyrazole ring of the another ligand with distance C20–H20B–Cg(3) is 2.872 Å and thus forming 1D chain along c-axis [Fig. 1(c)] [47,48].

For complex **2**, the four equatorial bond distances of Cu–N(2) [2.123(2) Å], Cu(1)–N(3) [1.988(2) Å], Cu(1)–N(6) [1.983(2) Å] and Cu(1)–Br(1) [2.3783(4) Å] are not same and apical position is occupied by secondary nitrogen N(1) with long Cu–N(1) [2.391(2) Å] distance. Deviations of coordinating atoms N(2), N(3), N(6) and Br(1) from the mean plane are 0.055, 0.010, 0.007 and 0.051 Å, respectively. For a square pyramidal structure, the copper(II) is slightly displaced 0.112 Å out of this mean square plane towards the secondary amine nitrogen of ligand bdpab. The chelate bite angles for three five membered chelate rings, N(1)–Cu(1)–N(2), N(2)–Cu(1)–N(3) and N(2)–Cu(1)–N(6) are 171.25(7), 79.85(10) and 82.26(10)°, respectively. These bond angles and distances are comparable with previously reported bromide and tripodal ligand containing copper(II) complex [49].

Two molecules in a unit cell are attached together through $\pi \dots \pi$ stacking between the two phenyl rings of two nearest ligand bdpab with distance between two centroids [Cg(1)–Cg(2)] is 4.027 Å and C–H... π interactions between one hydrogen atom of –CH₃ group attached with pyrazole ring and pyrazole ring of the nearest ligand with distance C11–H11c–Cg(3) is 2.936 Å and forming 1D chain along c-axis [Fig. 2(b)] [47,48].

3.3.2. Crystal structure of [Co(bdpab)(μ -Cl)]₂(PF₆)₂ (**5**)

The X-ray study revealed that dark pink crystal of complex **5** crystallize in triclinic system with *P*-1 space group [a = 9.6899 (3), b = 10.8074(5), c = 13.1823(5) Å] contain one dimeric [Co(bdpab)(μ -Cl)]⁺² cation. An ORTEP diagram of the dimeric cation with atomic labelling is shown in Fig. 3(a). Selected bond lengths and angles parameters are given in Table 2. Crystal structure of the complex shows that the complex consists of double chloride bridged dimer in which bridging Co₂Cl₂ is planar due to the presence of crystallographic inversion center in the middle of dimer.

In dimeric cation, both cobalt(II) centers are six coordinated and the geometry around Co(II) centers can be described as a distorted octahedral. Each cobalt atom is bonded to tetradentate ligand bdpab and remaining coordination sites are occupied by two bridging chloride ligands. Crystal structure shows that equatorial plane is occupied by three potential nitrogen donors N(2), N(3), N(5) and Cl(1i) from ligand and the remaining two axial positions are secured by one secondary nitrogen atom N(1) of the ligand and one chloride ion Cl(1). Ligand bdpab forms three ligand-metal-ligand chelate ring with bite angles varying between 76.35(6)° and 80.10(6)° and the rings are puckered so that the torsion angles of N(5)–N(6)–C(10)–N(2), N(2)–C(9)–N(4)–N(3) and N(2)–C(8)–C(7)–N(1) are 38.31°, 42.12° and 54.76°, respectively [50–51].

In complex **5**, the [Co(μ -Cl)₂Co] motif has been found in number of crystallographically characterised complexes and this motif is asymmetric because of Co–Cl bond lengths are 2.4786(5) and 2.4259(5) Å and the Co(1)–Cl(1)–Co(1i) bridging angle is 94.67°. The intra dimer cobalt–cobalt distance is 3.607 Å. These Co–Cl and Co...Co bond length values are compared with earlier reported chloride bridged cobalt complex [46].

In complex **5**, two binuclear molecules in unit cell are assembled by means of intermolecular face-to-face π - π interaction between phenyl ring and pyrazole ring of two nearest molecules with the centroid-centroid [Cg(1)–Cg(2)] distance is 4.260 Å [Fig. 3(b)] and the dihedral angle between them is 18.89° indicating a significant intermolecular face-to-face π - π stacking interaction. This π - π interaction forming 1D linear polymer along a-axis [47].

3.4. Antimicrobial activity

The Cu(II) and Co(II) complexes with the resolved structure viz. **1**, **3** and **5** and their ligands were studied for their antimicrobial activity against *Bacillus subtilis*, *Streptococcus aureus*, *Escherichia Coli* and *Pseudomonas aeruginosa* as shown in Table 3. No inhibition was observed in the negative control plate and strong inhibition in the presence of chloramphenicol proved the susceptibility of microorganisms to antimicrobial agents. Complexes **1** and **5** showed highest activity against gram positive microorganism with MIC of 5 mM against both *Bacillus subtilis* and *Streptococcus aureus*. In case of gram negative microorganisms, complex **3** displayed highest antimicrobial activity against *Escherichia coli* with MIC of 5 mM. Complex **3** and **5** equally inhibited *Pseudomonas aeruginosa* with MIC of 10 mM. Antimicrobial activity of cobalt(II) complex **5** was considerably consistent than copper(II) complexes **1** and **3**. A marked increase in the antimicrobial activity was exhibited on co-ordination of the metal ions with the ligand i.e. after complexation. The enhancement of the activity can be attributed to the presence of metal ions which influence the solubility, conductivity and dipole moment of the complexes which could be the significant factors responsible for increasing the penetration of the molecules into bacterial cell wall, effectively targeting the bacterial machinery by various mechanisms [52]. The antimicrobial activity data shows the copper(II) complexes with aromatic substituent bdpab ligand have higher activity than the previously reported similar complexes with N_4 -coordinate pyrazolyl ligand dbdmp with diethyl substituents [53,54].

3.5. Anti-proliferative activities of copper and cobalt salts and their complexes

The anti-proliferative activity of free ligand, copper and cobalt salts and their complexes were investigated against A549 lung carcinoma cancer cells. In the present study, all three salts and their complexes showed cytotoxicity. It was found that [Cu(bdpab)Cl]PF₆ and [Cu(bdpab)Br]PF₆ complexes showed maximum cytotoxicity compared to other complexes reported here and their respective salts [Fig. 5]. IC₅₀ value for the salts and their complexes CuCl₂·2H₂O, CuBr₂·4H₂O, CoCl₂·6H₂O, [Cu(bdpab)Cl]PF₆, [Cu(bdpab)Br]PF₆, [Co(bdpab)Cl]₂(PF₆)₂ and bdpab are 408.3, 314.2, 3119.18, 214.69, 68.34, 1089.8 and 601.028 µg/ml respectively. Metal salts are toxic and the ligand is nontoxic but showed potent cytotoxicity following its chelation with metal ions. Hence it can be concluded that the cytotoxic activity obtained with complexes are better than corresponding metal salts. Among the synthesized complexes, [Cu(bdpab)Br]PF₆ complex has best cytotoxic activity against human lung carcinoma cells.

Table 3
IC₅₀ and MIC activity data of the bdpab ligand, salts and complexes **1**, **3** and **5**.

Compounds	IC ₅₀ value (μg/ml)	MIC value in mM			
		<i>S. aureus</i>	<i>B. Subtilis</i>	<i>E. coli</i>	<i>P. aeruginosa</i>
CuCl ₂ ·2H ₂ O	408.3	>10	>10	10	>10
CuBr ₂ ·4H ₂ O	314.2	>10	>10	>10	>10
CoCl ₂ ·6H ₂ O	3119.18	10	10	10	10
bdpab	601.028	>10	>10	>10	10
[Cu(bdpab)Cl]PF ₆	214.69	5	5	10	>10
[Cu(bdpab)Br]PF ₆	68.34	10	10	5	10
[Co(bdpab)Cl] ₂ (PF ₆) ₂	1089.8	5	5	10	10

IC₅₀ i.e. half maximal inhibitory concentration, MIC i.e. minimum inhibitory concentration.

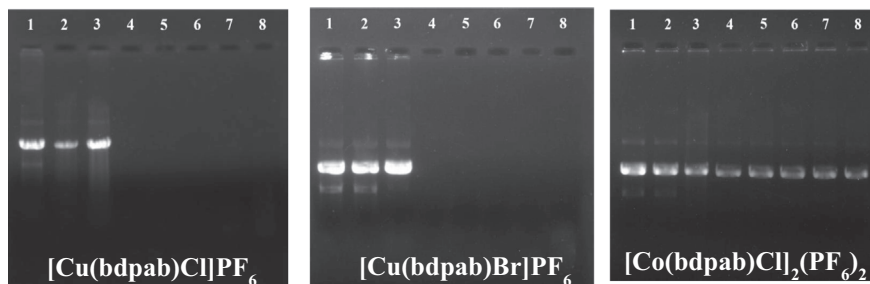


Fig. 4. Cleavage of DNA(pbs KS(+)) induced by complexes: Lane 1, untreated DNA; lane 2, plasmid DNA + 3 μl H₂O₂; lane 3, plasmid DNA + 50 μM complex; lane 4, plasmid DNA + 10 μM complex + 3 μl H₂O₂; lane 5, plasmid DNA + 20 μM complex + 3 μl H₂O₂; lane 6, plasmid DNA + 30 μM complex + 3 μl H₂O₂; lane 7, plasmid DNA + 40 μM complex + 3 μl H₂O₂; lane 8, plasmid DNA + 50 μM complex + 3 μl H₂O₂, respectively.

3.6. Cleavage experiment

In order to find out DNA cleavage activity of the synthesized compounds, the interaction of plasmid pBS KS(+) with the compounds in the presence of H₂O₂ was studied. The gel picture showing the cleavage of plasmid DNA by the complexes is depicted in [Fig. 4]. Thick bands were observed in the controls viz. untreated plasmid, plasmid with H₂O₂ only and plasmid with complex (50 μM) only in lane 1, lane 2 and lane 3 respectively. This suggested that the plasmid was intact without treatment and H₂O₂ and the complexes alone had no effect on the plasmid. The disappearance of the DNA bands after gel electrophoresis very clearly revealed that the complex **1** and **3** effectively cleaved the DNA even at the low concentration of 10 μM. In case of complex **5** the difference in the band thickness in controls and the treated samples was not much significant. The cleavage is thought to occur by the attack of free oxygen radicals produced by H₂O₂ on the DNA exposed after the treatment with the complexes [55]. On the basis of the results it is evident that the complex **1** and **5** are effective DNA cleavage

agents. The usage of DNA cleavage compounds range from cleavage at specific sites and complete digestion in molecular biology to targeted cleavage of cancer cell's DNA in chemotherapy and arresting the growth of pathogenic bacteria and viruses [56–58]. The copper complexes are being explored extensively for their use as chemical nucleases because they possess biologically accessible redox potential and relatively high nucleobase affinity [59–60].

4. Conclusion

Mononuclear copper(II) and binuclear cobalt(II) complexes have been synthesized with halide and tripodal N₄-coordinate ligand and characterized. Structural data show mononuclear copper complexes have square pyramidal and binuclear cobalt complex have octahedral geometry. Antimicrobial studies showed that all the tested complexes possess antimicrobial activity with complexes **1** and **5** are more effective against gram positive bacteria and complex **3** is more effective against gram negative bacteria. The complexes have complete DNA cleaving ability in presence of H₂O₂ even at very low concentrations. Cytotoxic activity of the complexes show copper complexes have cytotoxic activity and among the copper complexes, [Cu(bdpab)Br]PF₆ has highest activity. The molar conductivity values in acetonitrile of the mono- and dinuclear complexes are supporting 1:1 electrolyte. So the bioactivity data indicates that the dinuclear cobalt(II) complex disassembles in solution to render the corresponding mononuclear species which are responsible for the bioactivities.

Acknowledgements

Financial support from UGC, India in the form of major research project (F.No. 39-720/2010(SR)) is gratefully acknowledged. M. H. Sadhu thanks UGC, New Delhi for RGNF fellowship. We thank Dr. Pushpa Robin, Department of Biochemistry, The Maharaja Sayajirao University of Baroda, Vadodara, India for helpful discussion on bioactivities. The author acknowledges the use of Single Crystal

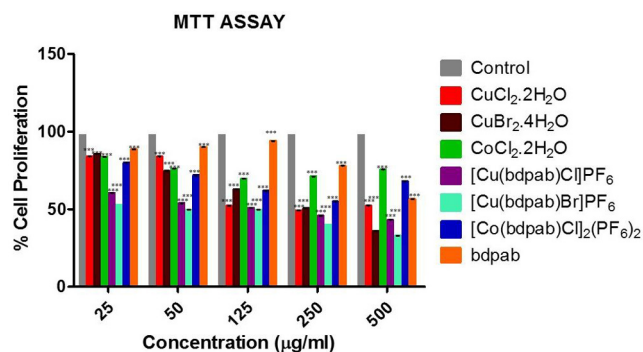


Fig. 5. Effect of Complexes exposed to A549 cells on cell viability. Data expressed as mean ± S.E.M. for n = 3. ***P < 0.001.

X-ray diffraction facility, DST-Purse program at Faculty of Science, The M. S. University of Baroda for crystallography study.

Appendix A. Supplementary data

CCDC 1529402, 1529364 and 1529365 contains the supplementary crystallographic data for **1**, **3** and **5**. These data can be obtained free of charge via <http://www.ccdc.cam.ac.uk/conts/retrieving.html>, or from the Cambridge Crystallographic Data Centre, 12 Union Road, Cambridge CB2 1EZ, UK; fax: (+44) 1223-336-033; or e-mail: deposit@ccdc.cam.ac.uk. Supplementary data associated with this article can be found, in the online version, at <http://dx.doi.org/10.1016/j.ica.2017.06.006>.

References

- [1] E.R. Jamieson, S.J. Lippard, *Chem. Rev.* 99 (1999) 2467.
- [2] L. Kelland, *Nat. Rev. Cancer* 7 (2007) 573.
- [3] C. He, C. Poon, C. Chan, S.D. Yamada, W. Lin, *J. Am. Chem. Soc.* 138 (2016) 6010.
- [4] R. Lincoln, Kohler, S. Monro, H. Yin, M. Stephenson, R. Zong, A. Chouai, C. Dorsey, R. Hennigar, R.P. Thummel, S.A. McFarland, *J. Am. Chem. Soc.* 135 (2013) 17161.
- [5] E.I. Solomon, P. Chen, M. Metz, S.K. Lee, A.E. Palmer, *Agnew. Chem. Int. Ed.* 40 (2001) 4570.
- [6] C. Santini, M. Pellei, V. Gandin, M. Porchia, F. Tisato, C. Marzano, *Chem. Rev.* 114 (2014) 815.
- [7] R. Ruiz, B. Garcia, J. Garcia-Tojal, N. Busto, S. Ibeas, J.M. Leal, C. Martins, J. Gaspar, J. Borrás, R. Gil-García, M.G. Alvarez, *J. Biol. Inorg. Chem.* 15 (2010) 515.
- [8] M.J. Wiester, P.A. Ulmann, C.A. Mirkin, *Angew. Chem. Int. Ed.* 50 (2011) 114.
- [9] F. Mancini, P. Scrimin, P. Tecilla, U. Tonellato, *Chem. Commun.* (2005) 2540.
- [10] X.-Q. Zhou, Q. Sun, L. Jiang, S.-T. Li, W. Gu, J.-L. Tian, X. Liu, S.-P. Yan, *Dalton Trans.* 44 (2015) 9516.
- [11] M. Alagesan, N.S.P. Bhuvanesh, N. Dharmaraj, *Dalton Trans.* 42 (2013) 7210.
- [12] S. Bhattacharyya, A. Sarkar, S.K. Dey, G.P. Jose, A. Mukherjee, T.K. Sengupta, *Dalton Trans.* 42 (2013) 11709.
- [13] L. Liu, G.M. Zhang, R.G. Zhu, Y.H. Liu, H.M. Yao, Z.B. Han, *RSC Adv.* 4 (2014) 46639.
- [14] P.R. Reddy, A. Shilpa, N. Raju, P. Raghavaiah, *J. Inorg. Biochem.* 105 (2011) 1603.
- [15] R. Ren, P. Yang, W.J. Zheng, Z.C. Hua, *Inorg. Chem.* 39 (2000) 5454.
- [16] Anbu, M. Kandaswamy, S. Kamalraj, J. Muthumarry, B. Varghese, *Dalton Trans.* 40 (2011) 7310.
- [17] A. Prisecaru, V. Mckee, O. Howe, G. Rochford, M. McCann, J. Collieran, M. Pour, N. Barron, N. Gathergood, A. Kellett, *J. Med. Chem.* 56 (2013) 8599.
- [18] S. Sathiyaraj, K. Sampath, G. Raja, R.J. Butcher, S.K. Gupta, C.J. Balakrishnan, *Inorg. Chim. Acta* 406 (2013) 44.
- [19] C.H. Ng, W.S. Wang, K.V. Chong, Y.F. Win, K.E. Neo, *Dalton Trans.* 42 (2013) 10233.
- [20] A.K. Patra, T. Bhowmick, S. Ramakumar, A.R. Chakravarty, *Inorg. Chem.* 46 (2007) 9030.
- [21] C. Fernandes, G.L. Parrilha, J.A. Lessa, L.J.M. Santiago, M.M. Kanashiro, F.S. Boniolo, A.J. Bortoluzzi, N.V. Vugman, M.H. Herbst, A. Horn Jr., *Inorg. Chim. Acta* 359 (2006) 3167.
- [22] K. Ghosh, P. Kumar, V. Mohan, U.P. Singh, S. Kasiri, S.S. Mandal, *Inorg. Chem.* 51 (2012) 3343.
- [23] T.W. Failes, C. Cullinane, C.I. Diakos, N. Yamamoto, J.G. Lyons, T.W. Hambley, *Chem. Eur. J.* 13 (2007) 2974.
- [24] K. Miyoshi, H. Tanaka, E. Kimura, S. Tsuboyama, S. Murata, H. Shimizu, K. Ishizu, *Inorg. Chim. Acta* 78 (1983) 23.
- [25] H. Gopinathan, N. Komathi, M.N. Arumugham, *Inorg. Chim. Acta* 416 (2014) 93.
- [26] E.V. Rybak-Akimova, A.Y. Nazarenko, L. Chen, P.W. Krieger, A.M. Herrera, V.V. Tarasov, P.D. Robinson, *Inorg. Chim. Acta* 324 (2001) 1.
- [27] W.L. Driessen, *Recl. Trav. Chim. Pays-Bas* 101 (1982) 441.
- [28] M.H. Sadhu, A. Solanki, S.B. Kumar, *Polyhedron* 100 (2015) 206.
- [29] J.-R. Guo, Q.-Q. Chen, C.W.-K. Lam, W. Zhang, *Biol. Res.* 48 (2015) 40.
- [30] H.C. Bimboim, J. Doly, *Nucl. Acids Res.* 7 (1979) 1513.
- [31] J. Marmur, *J. Mol. Biol.* 3 (1961) 208.
- [32] M.E. Reichmann, S.A. Rice, C.A. Thomas, P. Doty, *J. Am. Chem. Soc.* 76 (1954) 3047.
- [33] Agilent, CrysAlis PRO. Agilent Technologies UK Ltd, Yarnton, England, 2011.
- [34] G.M. Sheldrick, SAINT, 5.1 ed., Siemens Industrial Automation Inc., Madison, WI, 1995.
- [35] G.M. Sheldrick, SHELXL-97: Program for Crystal Structure Refinement, University of Göttingen, Göttingen, 1997.
- [36] L.J. Farrugia, *J. Appl. Cryst.* 32 (1999) 837.
- [37] L.J. Farrugia, *J. Appl. Crystallogr.* 30 (1997) 565.
- [38] W.J. Geary, *Coord. Chem. Rev.* 7 (1971) 81.
- [39] K. Nakamoto, *Infrared and Raman Spectra of Inorganic and Coordination Compounds*, 3rd ed., Wiley Interscience, New York, 1978.
- [40] U. Mukhopadhyay, I. Bernal, S.S. Massoud, F.A. Mautner, *Inorg. Chim. Acta* 357 (2004) 3873.
- [41] S.S. Massoud, F.A. Mautner, M.A.M. Abu-Youssef, N.M. Shuaib, *Polyhedron* 18 (1999) 2061.
- [42] B. Chakraborty, T.K. Paine, *Inorg. Chim. Acta* 378 (2011) 231.
- [43] J. Matsumoto, T. Suzuki, Y. Kajita, H. Masuda, *Dalton Trans.* 41 (2012) 4107.
- [44] A.W. Addison, T.N. Rao, J. Reedijk, J.V. Rijn, G.C. Verschoor, *J. Chem. Soc., Dalton Trans.* (1984) 1349.
- [45] Y. Funasako, M. Noshio, T. Mochida, *Dalton Trans.* 42 (2013) 10138.
- [46] R. Herchel, Z. Dvorak, Z. Travnicek, M. Mikuriya, F.R. Louka, F.A. Mautner, S.S. Massoud, *Inorg. Chim. Acta* 451 (2016) 102.
- [47] M.H. Sadhu, S.B. Kumar, *Polyhedron* 123 (2017) 419.
- [48] G. Aragay, D. Hernandez, B. Verdejo, E.C. Escudero-Adan, M. Martinez, P. Ballester, *Molecules* 20 (2015) 16672.
- [49] T.E. Patten, M.M. Olmstead, C. Troeltzsch, *Inorg. Chim. Acta* 361 (2008) 365.
- [50] C.J. Davies, G.A. Solan, J. Fawcett, *Polyhedron* 23 (2004) 3105.
- [51] S.B. Kumar, M. Zala, A. Solanki, M. Rangrez, P. Parikh, E. Suresh, *Polyhedron* 36 (2012) 15.
- [52] Z.H. Chohan, H. Pervez, A. Rauf, A. Scozzafava, C.T. Supuran, *J. Enzyme Inhib. Med. Chem.* 17 (2) (2002) 117.
- [53] A. Solanki, S.B. Kumar, A.A. Doshi, C. RatnaPrabha, *Polyhedron* 63 (2013) 147.
- [54] A. Solanki, M.H. Sadhu, S. Patel, R. Devkar, S.B. Kumar, *Polyhedron* 102 (2015) 267.
- [55] S. Tang, Y. Feng, Z. Xu, Y. Yang, D. Wang, *Asian J. Chem.* 25 (2013) 9237.
- [56] M. Pitie, C.J. Burrows, B. Meunier, *Nucl. Acids Res.* 28 (2000) 4856.
- [57] X. Lu, K. Zhu, M. Zhang, H. Liu, J. Kang, *J. Biochem. Biophys. Methods* 52 (2002) 189.
- [58] K.M. Vyas, R.G. Joshi, R.N. Jadeja, C. RatnaPrabha, V.K. Gupta, *Spectrochim. Acta Part A Mol. Biomol. Spectrosc.* 84 (2011) 256.
- [59] W.K. Pogozelski, T.D. Tullius, *Chem. Rev.* 98 (1998) 1089.
- [60] C.J. Burrows, J.G. Muller, *Chem. Rev.* 98 (3) (1998) 1109.